

# ScholarWorks@GSU

## Investigation and Characterization of Novel Pentamethine Cyanine Dyes for Use as Photosensitizers in Photodynamic Therapy

Authors	Kiernan, Kaitlyn
Citation	Kiernan, Kaitlyn. "Investigation and Characterization of Novel Pentamethine Cyanine Dyes for Use as Photosensitizers in Photodynamic Therapy." Thesis, Georgia State University, 2017. <a href="https://doi.org/10.57709/10059682">https://doi.org/10.57709/10059682</a>
DOI	<a href="https://doi.org/10.57709/10059682">https://doi.org/10.57709/10059682</a>
Download date	2026-05-15 17:53:35
Link to Item	<a href="https://hdl.handle.net/20.500.14694/3079">https://hdl.handle.net/20.500.14694/3079</a>

INVESTIGATION AND CHARACTERIZATION OF NOVEL PENTAMETHINE CYANINE  
DYES FOR USE AS PHOTSENSITIZERS IN PHOTODYNAMIC THERAPY

by

KAITLYN KIERNAN

Under the Direction of Kathryn B. Grant, Ph.D.

ABSTRACT

Cyanine dyes that absorb light in the near infrared to far red region of the electromagnetic spectrum are desirable as photosensitizers for photodynamic cancer therapy. Light of wavelengths in this range is able to deeply penetrate tissue allowing for practical *in vivo* use of these dyes. A series of three structurally similar pentamethine cyanine dyes that absorb light ~800 nm to ~500 nm was tested to determine the effects of structural influences on the yields of supercoiled DNA photo-converted to nicked or linear forms. Possible mechanisms and optimal parameters for near-quantitative DNA photocleavage with a symmetrical quinoline pentamethine cyanine dye are discussed.

INDEX WORDS: Photodynamic therapy, Cyanine dye, Reactive oxygen species, Gel electrophoresis, UV-visible spectrophotometry, DNA

INVESTIGATION AND CHARACTERIZATION OF PENTAMETHINE CYANINE DYES  
FOR USE AS PHOTSENSITIZERS IN PHOTODYNAMIC THERAPY

by

KAITLYN KIERNAN

A Thesis Submitted in Partial Fulfillment of the Requirements for the Degree of

Master of Science

in the College of Arts and Sciences

Georgia State University

2017

Copyright by  
Kaitlyn Kiernan  
2017

INVESTIGATION AND CHARACTERIZATION OF PENTAMETHINE CYANINE DYES  
FOR USE AS PHOTSENSITIZERS IN PHOTODYNAMIC THERAPY

by

KAITLYN KIERNAN

Committee Chair: Kathryn B. Grant

Committee: Maged Henary

Ming Luo

Electronic Version Approved:

Office of Graduate Studies

College of Arts and Sciences

Georgia State University

May 2017

## **DEDICATION**

I dedicate this thesis first and foremost to my mom who, without even knowing it, gave me the push to follow my heart, my dad for always being willing and eager to listen and encourage, and Steven, who lifts me up when things get tough and never lets me quit. I love you.

## ACKNOWLEDGEMENTS

I would like to start by acknowledging my advisor, Dr. Kathryn B. Grant, who's knowledge, advice, and support meant more than I can explain. Thank you for your continuous optimism and encouragement, even when times were tough. I am grateful to have had the opportunity to learn from you.

I'd also like to thank my all of my lab mates for making these two years not only knowledgeable but a whole lot of fun. You all made it exciting to come in to school every day and I am thankful to have made life-long friends out of all of you.

To the others who have given me more support and confidence than I deserve, Cory Holder, Kyle Emer, Andrew Puetz, you knew I could do this before I could convince myself and for that I am thankful.

## TABLE OF CONTENTS

ACKNOWLEDGEMENTS .....	v
LIST OF TABLES .....	viii
LIST OF FIGURES .....	ix
<b>1 INTRODUCTION .....</b>	<b>1</b>
<b>1.1 Cyanine Dyes .....</b>	<b>1</b>
<i>1.1.1 Structure and Stability of Cyanine Dyes .....</i>	<i>1</i>
<i>1.1.2 Aggregation .....</i>	<i>3</i>
<i>1.1.3 Interaction with DNA .....</i>	<i>4</i>
<b>1.2 Photodynamic Therapy .....</b>	<b>4</b>
<i>1.2.1 ROS Production .....</i>	<i>5</i>
<i>1.2.2 Photosensitizers .....</i>	<i>6</i>
<b>1.3 Summary of Research .....</b>	<b>9</b>
<b>2 EXPERIMENT .....</b>	<b>10</b>
<b>2.1 Materials and Instrumentation .....</b>	<b>10</b>
<b>2.2 Methods .....</b>	<b>11</b>
<i>2.2.1 UV-Visible Spectroscopy .....</i>	<i>11</i>
<i>2.2.2 Agarose Gel Preparation and Electrophoresis .....</i>	<i>11</i>
<i>2.2.3 Preliminary Photocleavage Gel Experiments .....</i>	<i>12</i>
<i>2.2.4 Concentration Optimization .....</i>	<i>12</i>

2.2.5	<i>Photocleavage Time Course Analysis</i> .....	13
2.2.6	<i>DNA Binding Studies</i> .....	13
2.2.7	<i>Scavenger Experiments</i> .....	14
3	<b>RESULTS</b> .....	16
3.1	<b>UV-Visible Screening for DNA Interactions and Dye Stability</b> .....	16
3.2	<b>Gel Electrophoresis</b> .....	21
3.2.1	<i>Determination of Optimal Light Source for Photocleavage</i> .....	21
3.2.2	<i>Concentration Titrations</i> .....	25
3.2.3	<i>Reaction Kinetics</i> .....	26
3.2.4	<i>ROS Scavengers</i> .....	28
3.3	<b>Binding Mode Investigation</b> .....	30
3.3.1	<i>UV-Visible Absorption Saturation</i> .....	30
3.3.2	<i>Circular Dichroism</i> .....	32
3.3.3	<i>UV-Visible Absorption Changes Induced by Pentamidine and Ethidium Bromide Addition</i> .....	35
4	<b>CONCLUSIONS</b> .....	37
	<b>REFERENCES</b> .....	40
	<b>APPENDICES</b> .....	42
	<b>Appendix A</b> .....	42
	<i>Appendix A.1</i> .....	42

**LIST OF TABLES**

Table 2.1 Order of sample addition to agarose gel for preliminary photocleavage experiments.	12
Table 2.2 Order of sample addition to agarose gel for concentration titration experiments .....	13
Table 2.3 Order of sample addition to agarose gel for scavenger experiments with sodium azide, sodium benzoate, catalase, and EDTA.....	15
Table 2.4 Order of sample addition to agarose gel for scavenger experiments with D <sub>2</sub> O.....	15
Table 3.1 Molar extinction coefficients and cleavage yields reported as % supercoiled DNA for dyes <b>1</b> , <b>2</b> , and <b>3</b> with lamps at 588 nm, 700 nm, 741 nm, and 850 nm.....	22

## LIST OF FIGURES

Figure 1.1 General Structure of Cyanine Dyes.....	1
Figure 1.2 Common heterocycles found as substituents on cyanine dyes.....	2
Figure 1.3 Structure of cyanine dyes used for this research synthesized by Cory Holder in Dr. Maged Henary's lab at Georgia State University. ....	2
Figure 1.4 Jablonski diagram.....	5
Figure 1.5 Fenton reaction for the generation of hydroxyl radical. <sup>15</sup> .....	6
Figure 1.6 Structures of some commercially available photosensitizers for PDT.....	9
Figure 3.1 UV-visible absorption spectra of 10 $\mu$ M concentration of dyes <b>1</b> , <b>2</b> , and <b>3</b> in DMSO recorded every 10 min for 30 min in a quartz cuvette .....	17
Figure 3.2 UV-Visible absorption spectra of 10 $\mu$ M dyes <b>1</b> , <b>2</b> , and <b>3</b> without and with 150 $\mu$ M CT-DNA in 10 mM sodium phosphate buffer pH 7.0 at t = 0.....	18
Figure 3.3 UV-Visible absorption spectra of 10 $\mu$ M dyes <b>1</b> , <b>2</b> , and <b>3</b> with and without 150 $\mu$ M bp of CT-DNA in 10 mM sodium phosphate buffer pH 7.0 recorded every 5 min over 30 min in a quartz cuvette.....	20
Figure 3.4 Gel electrophoresis pictures of 25 $\mu$ M dyes <b>1</b> , <b>2</b> , and <b>3</b> with 38 $\mu$ M b.p. of pUC19 plasmid DNA irradiated for 60 min under 700 nm (8 mW per LED), 850 nm (7.2 mW per LED), 588 nm (3 mW per LED), and 741 nm (180 mW per LED) light respectively (25 °C). ....	21
Figure 3.5 Temperature controlled gel electrophoresis experiment with 25 $\mu$ M of dyes <b>1</b> , <b>2</b> , and <b>3</b> , with 38 $\mu$ M bp of DNA, 10 mM of sodium phosphate buffer pH 7.0 at 10 °C with dark controls at 10 °C and 37°C irradiated at 741 nm with 180 mW of power for 1 h. ....	23

Figure 3.6 Gel electrophoresis experiment of dye <b>1</b> at 25 $\mu\text{M}$ concentrations in the presence of 38 $\mu\text{M}$ bp DNA and 10 mM sodium phosphate buffer pH 7.0 with dark controls at 45 $^{\circ}\text{C}$ and 37 $^{\circ}\text{C}$ to ensure that cleavage observed is due to the presence of light and not heat.....	24
Figure 3.7 Concentration titration gel electrophoresis experiments of dye <b>1</b> at varying concentrations with 38 $\mu\text{M}$ bp pUC19 plasmid DNA, 10 mM sodium phosphate buffer, pH 7.0, irradiated at 741 nm with a 180 mW LED lamp for 60 min at 10 $^{\circ}\text{C}$ .....	25
Figure 3.8 Gel picture of 24 $\mu\text{M}$ dye <b>1</b> in the presence of 38 $\mu\text{M}$ bp pUC19 plasmid DNA and 10 mM sodium phosphate buffer, pH 7.0, over time at 25 $^{\circ}\text{C}$ .....	27
Figure 3.9 reciprocal plot of concentration v. time showing the reaction order to be second order for 24 $\mu\text{M}$ of dye with 38 $\mu\text{M}$ bp DNA and 10 mM sodium phosphate buffer pH 7.0. Data points in red were excluded from the curve fitting procedure.....	28
Figure 3.10 Comparison of % inhibition of photocleavage by added chemical agents. Error over three trials is reported as standard deviation.....	29
Figure 3.11 UV-Visible absorption titration of 10 $\mu\text{M}$ dye <b>1</b> and increasing concentrations of CT-DNA in 10 mM sodium phosphate buffer, pH 7.0 .....	31
Figure 3.12 UV-visible and CD spectra of 10 $\mu\text{M}$ dye <b>1</b> with 646.23 $\mu\text{M}$ bp of CT-DNA in 10 mM sodium phosphate buffer pH 7.0 .....	33
Figure 3.13 CD absorption spectra of 10 $\mu\text{M}$ dye <b>1</b> , 646.23 $\mu\text{M}$ bp CT DNA, 10 mM sodium phosphate buffer, pH 7.0, from 450 to 200 showing the DNA unwinding upon the binding to dye <b>1</b> .....	34
Figure 3.14 UV-visible absorbance spectra to observe the effects of addition of 10 $\mu\text{M}$ pentamidine to a solution of 10 $\mu\text{M}$ dye <b>1</b> with 150 $\mu\text{M}$ bp CT-DNA and 10 mM sodium phosphate buffer.....	35

Figure 3.15 UV-visible spectra of EtBr with DNA to observe the effects of the addition of 10 $\mu\text{M}$ EtBr to DNA on dye <b>1</b> .....	36
Figure 0.1 Gel electrophoresis experiment to determine optimal concentration with dye <b>1</b> at high concentrations with 38 $\mu\text{M}$ bp DNA, and 10 mM sodium phosphate buffer, pH 7.0 irradiated with 741 nm light for 1 h in an ice bath at 10 $^{\circ}\text{C}$ . Lanes 1-4 are irradiated samples of dye <b>1</b> at 0, 12, 24, and 48 $\mu\text{M}$ , respectively and lanes 5-6 are dark controls. ....	42
Figure 0.2 Gel electrophoresis experiment to determine optimal concentration with dye <b>1</b> at low concentrations with 38 $\mu\text{M}$ bp DNA, and 10 mM sodium phosphate buffer, pH 7.0 irradiated with 741 nm light for 1 h in an ice bath at 10 $^{\circ}\text{C}$ . Lanes 1-4 are irradiated samples of dye <b>1</b> at 0, 3, 6, and 12 $\mu\text{M}$ , respectively and lanes 5-8 are dark controls. ....	43
Figure.0.3: Gel picture of photocleavage time course trial 2 with 24 $\mu\text{M}$ dye <b>1</b> , 38 $\mu\text{M}$ bp DNA, and 10 mM sodium phosphate buffer pH 7.0 with aliquots removed at $t=0, 5, 10, 30, 60, 100,$ and 120 min at 25 $^{\circ}\text{C}$ . Lane 9 is a dark control. ....	43
Figure 0.4 Gel picture of photocleavage time course trial 3 with 24 $\mu\text{M}$ dye <b>1</b> , 38 $\mu\text{M}$ bp DNA, and 10 mM sodium phosphate buffer pH 7.0 with aliquots removed at $t=0, 5, 10, 30, 60, 100,$ and 120 min at 25 $^{\circ}\text{C}$ .....	44
Figure 0.5 Second order kinetics plots trials 2 and 3 for 24 $\mu\text{M}$ dye <b>1</b> with 38 $\mu\text{M}$ bp DNA and 10 mM sodium phosphate buffer pH 7.0 at 25 $^{\circ}\text{C}$ . Red data points were excluded from the curve fitting.....	45
Figure 0.6 Sodium azide gel electrophoresis experiments with 24 $\mu\text{M}$ dye <b>1</b> , 38 $\mu\text{M}$ bp DNA, 100 mM sodium azide, and 10 mM sodium phosphate buffer pH 7.0 irradiated at 741 nm with a 180 mW lamp for 1 h.....	46

Figure 0.7 Sodium benzoate gel electrophoresis experiments with 24 $\mu\text{M}$ dye <b>1</b> , 38 $\mu\text{M}$ bp DNA, 100 mM sodium benzoate, and 10 mM sodium phosphate buffer pH 7.0 irradiated at 741 nm with a 180 mW lamp for 1 h.....	47
Figure 0.8 EDTA gel electrophoresis experiments with 24 $\mu\text{M}$ dye <b>1</b> , 38 $\mu\text{M}$ bp DNA, 100 mM EDTA, and 10 mM sodium phosphate buffer pH 7.0 irradiated at 741 nm with a 180 mW lamp for 1 h.....	48
Figure 0.9 Catalase gel electrophoresis experiments with 24 $\mu\text{M}$ dye <b>1</b> , 38 $\mu\text{M}$ bp DNA, 100 U/ $\mu\text{L}$ catalase, and 10 mM sodium phosphate buffer pH 7.0 irradiated at 741 nm with a 180 mW lamp for 1 h.....	49
Figure 0.10 D <sub>2</sub> O gel electrophoresis experiments with 24 $\mu\text{M}$ dye <b>1</b> , 38 $\mu\text{M}$ bp DNA, 72% (v/v) D <sub>2</sub> O, and 10 mM sodium phosphate buffer pH 7.0 irradiated at 741 nm with a 180 mW lamp for 1 h.....	50

## 1 INTRODUCTION

### 1.1 Cyanine Dyes

The discovery of cyanine dyes by Greville Williams in 1856 is believed to be one of the earliest reports of a synthetic, non-naturally occurring dye. Named for the color blue, these dyes actually absorb light from the ultraviolet to the infrared wavelength regions of the electromagnetic spectrum, giving them a broader range of colors than any other class of dye.<sup>1</sup> Too unstable in light to be used on fabrics, these dyes found applications as photosensitizers for silver halide photography to make panchromatic film. Cyanines have also been used in optical recording disks such as CDs and DVDs.<sup>2</sup>

More recently, cyanine dyes have gained popularity as near infrared fluorescent probes used for imaging and detection in biological systems. The dyes' quantum yields and high molar extinction coefficients make them good fluorophores for biological imaging.<sup>3</sup> These properties that make these dyes desirable for fluorescent imaging, stem from the extended conjugation present throughout the dye molecule.

#### 1.1.1 Structure and Stability of Cyanine Dyes

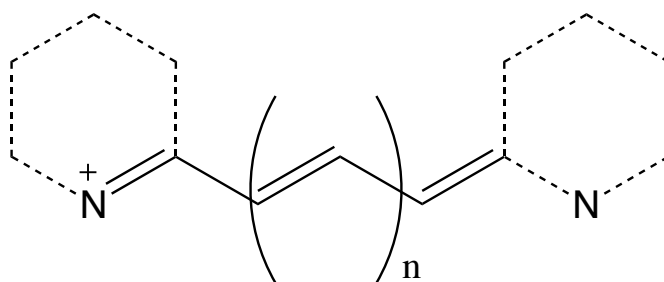


*Figure 1.1 General Structure of Cyanine Dyes*

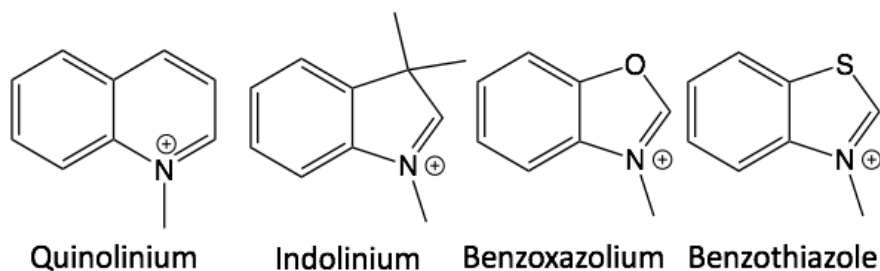


*Figure 1.2 Common heterocycles found as substituents on cyanine dyes.*

The general structure of cyanine dyes can be described as two nitrogen containing heterocycles bridged by a polymethine chain (Figure 1.1). This conjugation has effects on dye stability and absorption, in different solvents by delocalization of the nitrogen's positive charges throughout the entire molecule.<sup>2</sup> Resonance created by this conjugation results in stabilization of the dye. The some common heterocycles seen in cyanine dyes are benzoxazolium, quinolinium, indolium, and benzothiazole ring systems (Figure 1.2).<sup>4</sup> The structure of cyanine dyes can also be modified by changing the length of the polymethine bridge and its substituents.

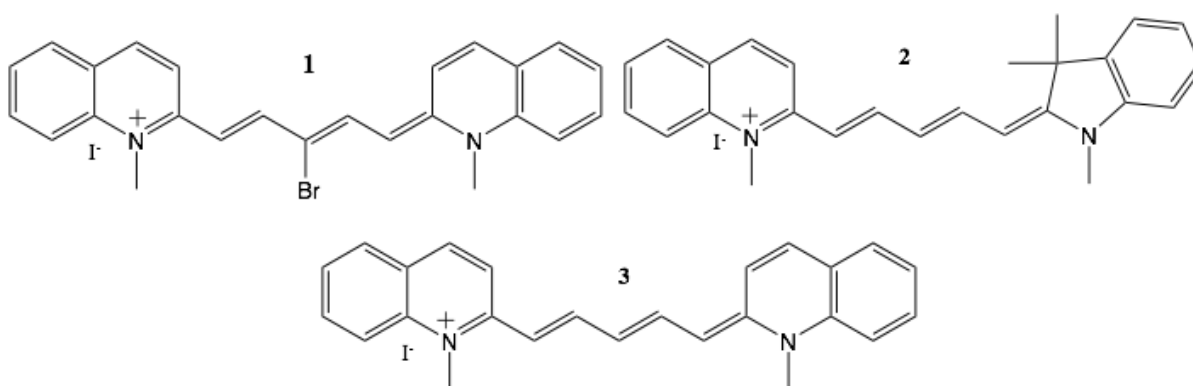


*Figure 1.3 Structure of cyanine dyes used for this research synthesized by Cory Holder in Dr. Maged Henary's lab at Georgia State University.*

Modification of the structure of these dyes allows for researchers to design new cyanines for specific purposes. For example, adding a double bond to the polymethine bridge the absorption

spectrum of the dye will shift  $\sim 100$  nm towards the red.<sup>5</sup> Adding electron withdrawing groups to the *meso* position of the molecule may increase the dye's stability by protecting the molecule from autoxidation.<sup>6</sup>

An issue with some cyanine dyes is their tendency towards photodegradation. This occurs in the presence of molecular oxygen and light. When the dye absorbs light, it reacts with surrounding oxygen to form singlet oxygen, a reactive oxygen species (ROS). These ROS are then able to react with the dye molecule itself, resulting in its degradation.<sup>6</sup> This can be avoided by structural modifications such as added rigidity.<sup>7</sup>

The dyes of focus in this research consist of a dye with either symmetrical quinoline rings and a pentamethine bridge with a bromine substituent in the *meso* position (**1**), an asymmetrical dye with one quinoline ring, one indole ring, and a pentamethine bridge with a proton in the *meso* position (**2**), or a dye with symmetrical quinoline rings and pentamethine bridge with a proton in the *meso* position (**3**) (Figure 1.3).

### **1.1.2 Aggregation**

In polar solvents, cyanine dyes have been shown to have a tendency to self-aggregation due to the planar  $\pi$ - $\pi$  stacking of the molecules.<sup>7</sup> Aggregation of these dyes is placed in two categories dependent on the molecular angle of slippage.<sup>8</sup> H-aggregates and J-aggregates vary in their geometries with H-aggregates having a vertically stacked pattern and J-aggregates having a staircase arrangement. This leads to spectral differences between the monomer dye, J aggregates, and H aggregates with the H-aggregates having a blue shift and J-aggregates having a red shift relative to the monomeric form. The presence of each aggregate is dependent on various factors including pH, concentration, solvent polarity, and ionic strength.<sup>9</sup> The more nonpolar the dye the more aggregation will form in polar solvents. Thus the structure of the dye will affect its

aggregation. It is suggested that molecules with hydrogen substituents have a tendency towards H-aggregation while the longer the polymethine bridge, the more likely the dye will form J-aggregates. Thus, dyes with more extended planar ring systems and longer polymethine bridges have been shown to exhibit increased self-aggregation.<sup>10</sup> Concentration effects aggregation as H-aggregates tendency for cooperativity.<sup>11</sup> Ionic strength of solution leads dyes to aggregate due to changes in electrostatic interactions.<sup>4</sup>

### ***1.1.3 Interaction with DNA***

Cyanine dyes are able to interact with DNA in various ways. They can position themselves in between base pairs through intercalation, bind within the minor groove, or bind externally to the molecule depending on the structure of the dye. Their positive charge allows them to interact with the negatively charged phosphate backbone of DNA creating an electrostatic attraction between the dye and DNA.<sup>4</sup> Intercalation is seen frequently with cyanine dyes because of their planar aromatic rings.<sup>2,4</sup> Groove binders must be able to twist around the helix of DNA, requiring less rigidity in the dye.<sup>4</sup> Binding modes of specific cyanine dyes can be determined through biophysical instrumentation including UV-visible, circular dichroism, and fluorescence spectroscopies.

## **1.2 Photodynamic Therapy**

In recent years, cyanine dyes have been studied as photosensitizers (PS) for photodynamic therapy (PDT).<sup>12</sup> PDT is a less invasive cancer therapy that employs a PS and light to produce highly unstable reactive oxygen species (ROS). Utilization of a PS that binds to DNA ensures that the short-lifetime ROS are damaging targeted cancer cells and not the surrounding healthy tissue.<sup>13</sup> This leads to ideal outcomes for patients with concerns about long recovery times or cosmetic side effects associated with other therapies. PDT can be combined with other common treatments for

cancer such as chemotherapy and radiation without any loss in sensitivity of PDT, allowing for more aggressive treatments. Ideal PS do not linger in the cells, ensuring that no therapeutically resistant DNA mutations are formed. As a primarily outpatient procedure, PDT is efficient in treatment, cost, and time.<sup>12</sup>

### 1.2.1 ROS Production

As mentioned earlier, the mechanism for PDT is a relatively simple one. A PS is injected into the targeted tumor or lesion. Then, light is applied to the area for a specific amount of time in order to allow the PS to become excited to its singlet energy state  $S_1$  (Figure 1.4).<sup>14</sup> At this point, an excited molecule has a few pathways it can travel for relaxation. In order to be an effective PS, the quantum yield of intersystem crossing to the  $T_1$  triplet state transition must be high.<sup>15</sup> In other words, the non-radiative transition from the  $S_1$  excited singlet state to the lower  $T_1$  energy triplet state should be faster than the other modes of relaxation such as fluoresce.<sup>13</sup>

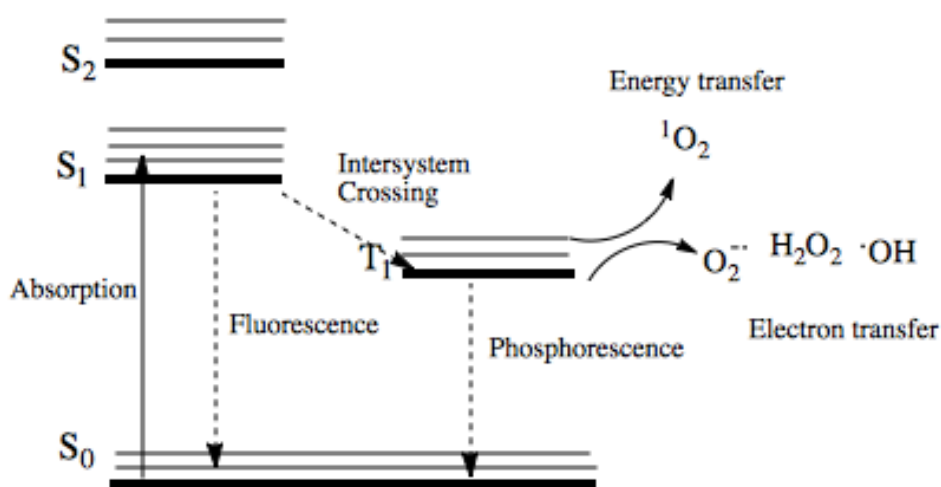
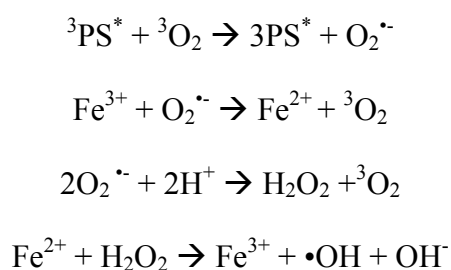


Figure 1.4 Jablonski diagram.

From the triplet state, the excited PS can react with surrounding molecular oxygen in two different ways to create ROS. Type II reactions involve the transfer of energy from PS to molecular

oxygen ( $^3\text{O}_2$ ), generating singlet oxygen ( $^1\text{O}_2$ ). Type I reactions are electron transfer reactions from PS to molecular oxygen to ground state molecular oxygen. The type I reaction is able to form hydrogen peroxide ( $\text{H}_2\text{O}_2$ ) and hydroxyl radicals ( $\bullet\text{OH}$ ) from superoxide ( $\text{O}_2^{\bullet-}$ ) anions through Fenton chemistry (Figure 1.5).<sup>16</sup>

In order for PDT to be effective, the PS must be activated by light in the near infrared to infrared region of the electromagnetic spectrum. At wavelengths from 700 nm to 900 nm,



*Figure 1.5 Fenton reaction for the generation of hydroxyl radical.*<sup>15</sup>

light is able to penetrate deeper through biological tissue due to the decrease in absorption and light scattering in this region.<sup>17</sup> At wavelengths above 900 nm the energy is not sufficient for the production of ROS needed to cause damage to tumor cells.<sup>17</sup>

## **1.2.2 Photosensitizers**

### **1.2.2.1 Ideal Photosensitizer**

The discovery of an ideal photosensitizers is an important focus of PDT. As research on this treatment has progressed, it has been realized that the current photosensitizers available on the market are not fulfilling all of the requirements that would ensure an ideal PS reagent. In order to be successful as a PS, a compound must meet three essential parameters: (i) low toxicity in the dark, in healthy tissue, and after being metabolized, (ii) absorption of light in the biological window, and (iii) rapid elimination from the patient after treatment.<sup>18</sup> Low dark toxicity ensures

that only the target cells are damaged, preserving the reputation of PDT as a treatment with low side effects. It is also necessary for an ideal PS to absorb closest to the middle of the region of 700 nm to 900 nm because, as mentioned earlier, this ensures that the light can penetrate biological tissue deeply without losing the energy needed to convert ground state oxygen into damage-inducing ROS<sup>19, 20</sup>

In addition to the three essential parameters, there are a few more that contribute to making an ideal photosensitizer. Having a photosensitizing compound with a high molar extinction coefficient and a high triplet state quantum yield will aid in the efficiency of a PS. As with most drugs, it is important to keep in mind amount of material and costs. A compound with a higher molar extinction coefficient will absorb more light at lower concentrations. This parameter allows the utilization of cost efficient materials. A high triplet state quantum yield comes about if the rate of converting ground state oxygen to its excited triplet state is faster than the rates of relaxation of the excited PS to its ground state through pathways such as fluorescence and phosphorescence<sup>19</sup>.

#### ***1.2.2.2 Commercially Available Photosensitizers***

As of now there are few commercially available PS on the market with only one of them being a cyanine dye (Figure 1.6). The oldest and most well-known clinically used PS is Photofrin<sup>®</sup> from Axcan Pharma, Inc. This compound is derived from hematoporphryn. Photofrin<sup>®</sup> now has many derivatives that have become commercially available and used clinically as well. This drug is predominantly used for lesions having to do with the lungs and esophagus and also as a treatment for bladder cancer, squamous cell, basal cell, and breast cancers.<sup>18</sup> Although this drug has found a wide variety of promising applications, it also has some drawbacks that encourage the discovery of more efficient photosensitizers. Photofrin<sup>®</sup> causes sensitivity to light in its patients, requiring them to avoid sun exposure for a minimum of four weeks.<sup>20, 21</sup> There is also an issue with

Photofrin's<sup>®</sup> absorption peak being close to the lower end of the biological window, making it inefficient in targeting tumors that are deep tissue. In the same porphyrin family are other clinically studied PS such as ALA or 5-Aminolevulinic acid, used for basal cell and squamous cell cancers.<sup>18</sup> Applied topically, this drug does not penetrate far into tissue. Methyl aminolevulinate (MAL) absorbs at 635 nm and is used to treat cancer of the throat.<sup>15</sup> Other clinically used PS include temoporfin absorbing at 652 nm which is used to treat squameous cell cancers of the head and neck.<sup>22</sup> Verteporfin is a PDT agent that absorbs at 689 nm and is used to treat age related macular degeneration which can cause blindness.

Indocyanine green (ICG) began as a fluorescent imaging label but recently has been modified to function as a PDT PS on its own. Its effectiveness at being a fluorophore limits its use as a PS because of the low quantum yield of intersystem crossing to the triplet state. Modifications to ICG by addition of iodine atoms performed by Atchison et. al. increased the dye's triplet state quantum yield, allowing for the use of modified ICG as a PS in PDT.<sup>23</sup>

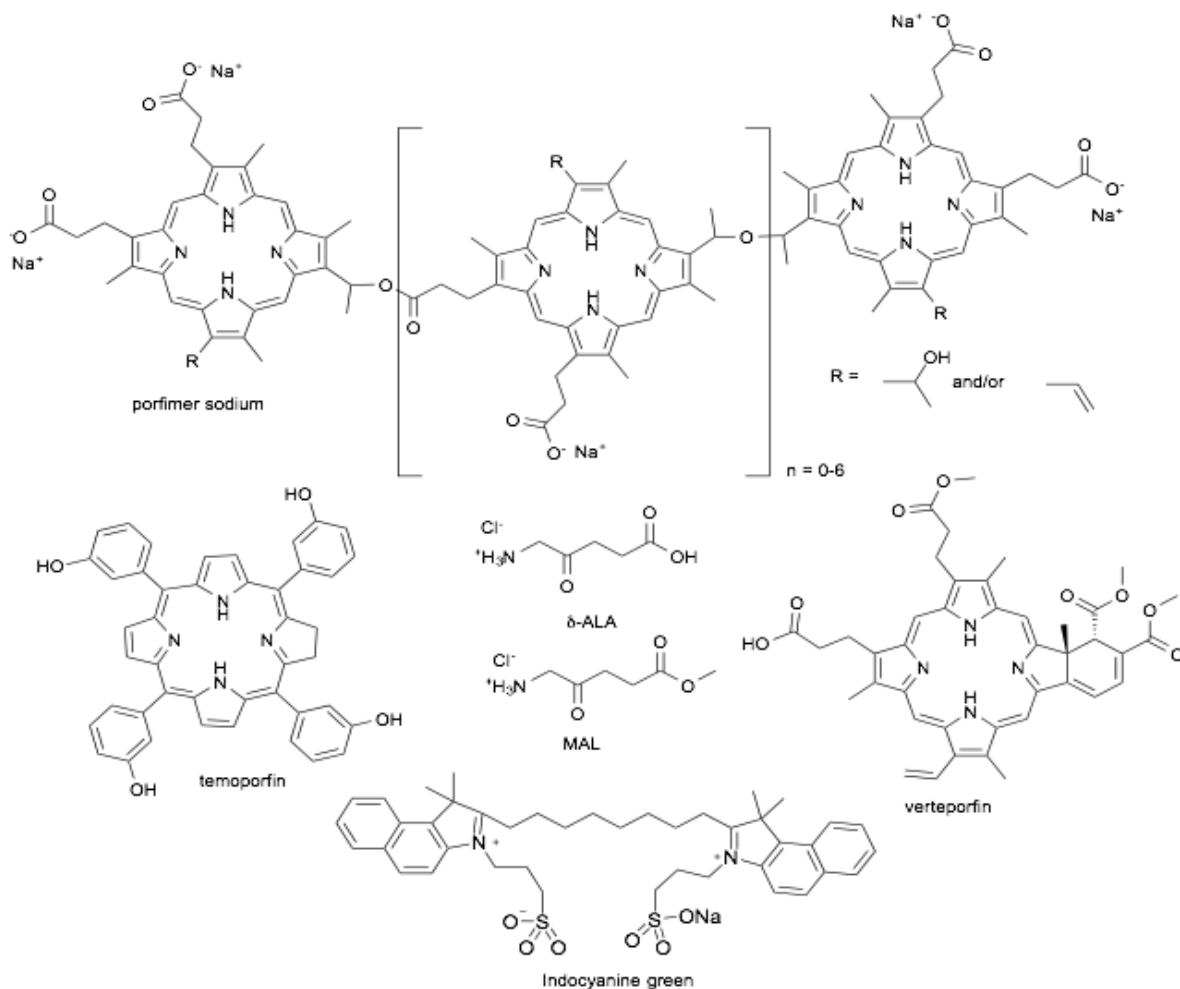


Figure 1.6 Structures of some commercially available photosensitizers for PDT

### 1.3 Summary of Research

The work described in this thesis focuses on a series of three cyanine dyes (Figure 1.3) synthesized by Dr. Maged Henary's lab at Georgia State University. The dyes were studied for their ability to serve as DNA photosensitizers for PDT. Because of their absorption in the near IR range, these dyes began by satisfying one of the parameters for an ideal PS. Dye **1** was determined to be stable in aqueous solution in the presence of DNA and efficient at converting supercoiled pUC19 plasmid DNA into its nicked and linear forms upon irradiation with a 180 mW per LED 741 nm medical lamp. To further investigate the features of this dye, its binding mode was studied by circular dichroism to observe any changes in the DNA CD signal when combined with

compound and any induced CD spectral features resulting from the binding of chiral DNA to the achiral dye. UV-visible spectra were utilized to compare the ability of dye **1** to bind to DNA in the presence of a known intercalator and minor groove binder. Then, several experiments were performed to test for the ROS involvement in the DNA photocleavage reaction.

## 2 EXPERIMENT

### 2.1 Materials and Instrumentation

For all experiments, water was deionized and distilled. Sodium phosphate buffer (pH 7.0) was prepared from monobasic and dibasic sodium phosphate from Fischer Scientific (Fairlawn, NJ). Cyanine dyes were synthesized and purified by Cory Holder in the Henary Lab (Georgia State University). Calf thymus (CT) DNA supplied by Invitrogen (Lot no. 780948, 10 mg/mL). Agarose was obtained from BioRad (Herclues, CA) and Fischer Scientific (Fairlawn, NJ). The pUC19 plasmid DNA was prepared using transfected *E. coli* competent cells (Stratagene, XL-1 blue) cloned in bacterial cultures and purified using the QIAfilter Plasmid Mega Kit (Qiagen™, Cat no. 12263). Ethidium bromide (EtBr), dimethyl sulfoxide (DMSO), sodium chloride, and methanol were purchased from Sigma-Aldrich (St. Louis, MO). Ethylenediaminetetraacetic acid disodium salt (EDTA) was purchased from IBI Scientific (Peosta, IA) and tris(hydroxymethyl)aminomethane (tris base) from Research Product International (Mt. Prospect, IL). Sodium azide ( $\geq 99.9\%$ ), sodium benzoate (99%), D<sub>2</sub>O, pentamidine isethionate salt, and catalase from bovine liver were all purchased from Sigma-Aldrich (St. Louis, MO).

UV-visible spectra were recorded using a PerkinElmer Lambda 35 UV/VIS spectrophotometer with samples in a quartz cuvette. DNA photocleavage experiments utilized light emitting diode-containing bar lamps with emission wavelengths of 588 nm (3 mW per LED),

700 nm emission (8 mW per LED), 850 nm emission (7.2 mW per LED) as well as a medical lamp with a maximum emission of 741 nm and a spectral output range of 707 nm to 759 nm (180 mW per LED). DNA electrophoresis was conducted in a gel box from Bio-Rad with a current of 100 mV applied by a GIBCO BRL electrophoresis power supply (Life Technologies). After electrophoresis, gels were visualized at 302 nm using a transilluminator from VWR Scientific and photographed using a digital camera equipped with the UVP PhotoDoc-It™ imaging system. A Jasco J-810 spectropolarimeter was used to record circular dichroism (CD) spectra in a 3 mL quartz cuvette.

## **2.2 Methods**

### ***2.2.1 UV-Visible Spectroscopy***

UV-visible spectra of each compound were recorded from 1100 nm to 200 nm, first in a DMSO solution with no CT-DNA present, then in an aqueous 10 mM sodium phosphate pH 7.0 solutions, every 5 min for 30 min in the absence and presence of CT-DNA. The concentration of dye was constant at 10  $\mu$ M (from a 500  $\mu$ M substock in DMSO), DNA at 150  $\mu$ M base pairs (bp), and buffer at 10 mM through all experiments. Cuvettes held a total sample volume of 600  $\mu$ L. Spectra of each dye in aqueous solutions and were compared to determine dye stability over time with and without DNA, and to observe any shifts and/or aggregation in the spectra caused by the DNA addition.

### ***2.2.2 Agarose Gel Preparation and Electrophoresis***

For electrophoresis experiments, a 1.5% agarose gel was prepared by dissolving 1.5 g agarose in 100 mL of 1 x TAE buffer pH 7.0, in a 500 mL Erlenmeyer flask in the microwave until homogeneous. A total of 10  $\mu$ L EtBr (5  $\mu$ g/mL) was added and the agarose was poured into a gel cast and left to harden for 1 h. After solidifying, the gel was moved to a gel box and submerged in

650 mL of 1 x TAE buffer with an additional 10  $\mu$ L of EtBr. A total of 3  $\mu$ L of loading buffer (15% (w/v) Ficoll and 0.025% (w/v) Bromophenol Blue) was added to the samples and allowed to equilibrate for a short period of time. Then, 20  $\mu$ L aliquots of the samples were loaded into the gel wells. Upon electrophoresis, DNA moved from the negative electrode to positive electrode through the gel, which resulted in its separation based on size and conformation.

### 2.2.3 Preliminary Photocleavage Gel Experiments

Three LED bar lamps were tested: 588 nm with a power of 3 mW per LED, 700 nm with a power of 8 mW per LED, and 850 nm with a power of 7.2 mW per LED. Then, a medical lamp was tested with an emission maximum of 741 nm and spectral output between 707 and 759 nm and a power of 180 mW per LED. To test the efficiency of each lamp, dyes **1**, **2**, and **3** were irradiated for 1 h. Samples consisted of 25  $\mu$ M dye, 10 mM sodium phosphate buffer (pH 7.0), ddH<sub>2</sub>O and 38  $\mu$ M bp of pUC19 plasmid DNA with a final volume of 30  $\mu$ L. After irradiation, 20  $\mu$ L of samples were loaded into the 1.5% agarose gel and electrophoresed with a current of ~100 V for 1 h (Table 2.1).

<b>Dye</b> ( $\mu$ M)	-	-	<b>1</b>	<b>2</b>	<b>3</b>	<b>1</b>	<b>2</b>	<b>3</b>
<b>DNA</b>	+	+	+	+	+	+	+	+
<b>Light</b>	-	+	+	+	+	-	-	-

Table 2.1 Order of sample addition to agarose gel for preliminary photocleavage experiments.

### 2.2.4 Concentration Optimization

Concentrations of dye **1** between 0  $\mu$ M and 48  $\mu$ M were tested in samples consisting of 38  $\mu$ M bp pUC19 plasmid DNA, 10 mM phosphate buffer (pH 7.0), and ddH<sub>2</sub>O. Total sample volumes were 30  $\mu$ L. After 1 h of irradiation at 741 nm with a 180 mW lamp, samples were then

loaded into the 1.5% agarose gel and run as previously described for 1 h (Table 2.2). These experiments were performed at 10 °C in which the reactions were set in a metal block equilibrated in the ice bath. A thermometer inserted into the block was used to monitor temperature

<b>Dye (<math>\mu\text{M}</math>)</b>	0	12	24	48	0	12	24	48
<b>DNA</b>	+	+	+	+	+	+	+	+
<b>Light</b>	+	+	+	+	-	-	-	-

Table 2.2 Order of sample addition to agarose gel for concentration titration experiments

### 2.2.5 Photocleavage Time Course Analysis

This experiment was done by irradiation of a large sample containing 24  $\mu\text{M}$  dye **1**, 10 mM sodium phosphate buffer, pH 7.0, and 38  $\mu\text{M}$  bp pUC19 plasmid DNA. The total sample volume was 210  $\mu\text{L}$  in a plastic cuvette. Individual 30  $\mu\text{L}$  aliquots were removed from this sample after  $t = 0$  min, 5 min, 10 min, 30 min, 60 min, 80 min, 100 min, and 120 min of irradiation. The 741 nm lamp was placed so the light would travel through the side of the cuvette ensuring that the entirety of the sample was exposed to the light in the same manner while maintaining irradiation as portions were removed. The DNA samples were then loaded into the wells of an agarose gel and resolved at 100 V for 1 h. Samples were kept at 25 °C.

### 2.2.6 DNA Binding Studies

In order to determine the binding mode of dye **1** with DNA, circular dichroism was utilized to observe if addition of DNA, a chiral molecule, to the achiral dye molecule would lead to an induced CD spectrum and/or a change in DNA CD peaks. In order to estimate the concentration of CT-DNA needed to completely bind 10  $\mu\text{M}$  of dye **1**, we monitored the change in dye absorbance with increasing amounts of CT-DNA. In a quartz cuvette, 10  $\mu\text{L}$  of dye **1**, from a DMSO stock concentration of 500  $\mu\text{M}$ , was combined with 50  $\mu\text{L}$  sodium phosphate buffer pH

7.0, and 440  $\mu\text{L}$  of ddH<sub>2</sub>O for a total sample volume of 500  $\mu\text{L}$ . The starting concentrations were 10  $\mu\text{M}$  of dye **1** and 10 mM of sodium phosphate buffer. An initial spectrum was recorded to observe the dye in the absence of CT-DNA. Next, CT-DNA was added in 2  $\mu\text{L}$  increments and spectra were recorded after each addition. Saturation was reached when absorbance of dye no longer changed, indicating that all of the dye molecules were bound to the DNA.

Using the optimal CT DNA concentration determined by UV-visible spectrophotometry, circular dichroism spectra were recorded for the dye **1**, CT-DNA, and dye **1** and CT-DNA from 850 nm to 200 nm. In a 3 mL quartz cuvette samples contained 10  $\mu\text{M}$  dye **1**, 10 mM sodium phosphate buffer pH 7.0, 646.23  $\mu\text{M}$  bp of CT-DNA, and ddH<sub>2</sub>O with a total volume of 1.5 mL. Samples were scanned over 12 accumulations from 200 nm to 850 nm with a scan speed of 200 nm/min and a band width of 0.5 nm.

### **2.2.7 Scavenger Experiments**

All scavenger experiments were performed in triplicate. The gel pictures were quantitated using the ImageQuant v.5.2 software and % inhibition was calculated for each trial and averaged using the formula

$$\left[ (\% \text{ nicked} + \% \text{ linear})_{\text{without reagent}} - (\% \text{ nicked} + \% \text{ linear})_{\text{with reagent}} \right] / (\% \text{ nicked} + \% \text{ linear})_{\text{without reagent}}$$

#### **2.2.7.1 Sodium Azide and Sodium Benzoate**

For these experiments, 5  $\mu\text{L}$  of 800 mM stock of inhibitor in ddH<sub>2</sub>O for a concentration of 100 mM was added to a sample of 24  $\mu\text{M}$  dye **1**, 10 mM sodium phosphate buffer, and 38  $\mu\text{M}$  bp of pUC19 plasmid DNA with a total sample volume of 40  $\mu\text{L}$ . The samples were given 1 min to equilibrate and then irradiated under the 741 nm medical lamp for 60 min. After irradiation, samples were loaded into the wells of a 1.5% agarose gel and run at 100 V for 1 h (Table 2.3). The gel was then visualized on the UVP-Photodock-it imaging system.

DNA	+	+	+	+	+	+	+
Dye	-	-	+	+	+	-	+
Reagent	-	+	-	-	+	-	+
Light	+	+	-	+	+	-	-

*Table 2.3 Order of sample addition to agarose gel for scavenger experiments with sodium azide, sodium benzoate, catalase, and EDTA*

### 2.2.7.2 Deuterium Oxide

Photocleavage reactions containing 24  $\mu\text{M}$  dye **1**, 38  $\mu\text{M}$  b.p. pUC19 plasmid DNA, and 10 mM sodium phosphate buffer were prepared in 72% (V/V)  $\text{D}_2\text{O}$ . After a 1 min equilibration period, samples were irradiated for 60 min and then electrophoresed at 100 V for 60 min on a 1.5% agarose gel.

DNA	+	+	+	+	+
Dye	-	+	+	+	+
$\text{D}_2\text{O}$	+	-	+	+	-
Light	+	-	-	+	+

*Table 2.4 Order of sample addition to agarose gel for scavenger experiments with  $\text{D}_2\text{O}$*

### 2.2.7.3 EDTA

EDTA is a well-known metal chelator and was used to test for the involvement of trace metals in solution in the photocleavage reactions. A total of 8  $\mu\text{L}$  of a 500 mM solution of EDTA pH 8.0 was added to samples containing 24  $\mu\text{M}$  dye **1**, 38  $\mu\text{M}$  bp pUC19 plasmid, and 10 mM sodium phosphate buffer, pH 7.0, giving a final concentration of 100 mM EDTA and a total sample volume of 40  $\mu\text{L}$ . The 741 nm medical lamp was then used for irradiation of these samples for 60 min.

#### **2.2.7.4 Catalase**

Adding catalase to samples before irradiation of light is a method to detect the involvement of hydrogen peroxide in the mechanism of DNA photocleavage. For these experiments, 100 U/ $\mu$ L was added to a sample containing 38  $\mu$ M bp pUC19 plasmid DNA, 10 mM sodium phosphate buffer pH 7.0, and 24  $\mu$ M dye **1** 40  $\mu$ L final volume. A decrease in the amount of supercoiled pUC19 being transformed into its nicked and linear form would signal the involvement of H<sub>2</sub>O<sub>2</sub> in the photocleavage reaction.

### **3 RESULTS**

#### **3.1 UV-Visible Screening for DNA Interactions and Dye Stability**

To begin understanding how cyanine dyes **1**, **2**, and **3** would behave, in solution UV-visible spectroscopy was used for initial studies. Spectra were recorded over time in DMSO and in aqueous solutions in the presence and absence of CT-DNA. DMSO spectra revealed whether the dye in question would remain stable while being stored in DMSO. Spectra from aqueous solutions at pH 7.0 to observe behaviors over time were necessary to mimic biological conditions where these dyes would be utilized as photosensitizers. It is important to note whether or not the absorbance of each dye is decreasing or remaining stable in aqueous solutions, specifically when DNA is present. Aside from observing the absorbance changes over time, it was also necessary to observe any shifts in spectra as these may be indicative of aggregation and/or interactions between the dye and DNA molecules. The spectra in Figure 3.1 clearly shows that dyes **1**, **2**, and **3** are stable over time in DMSO. These spectra can serve as a reference for these dyes as newly made stock solutions are prepared to assure the quality of the new working solutions. A symmetrical

indole quinoline dye **2** absorbed light much more strongly than symmetrical quinoline dyes **1** and **3**. The maximum absorption is 693 nm for dye **1**, 654 nm for dye **2**, and 715 nm for dye **3**.

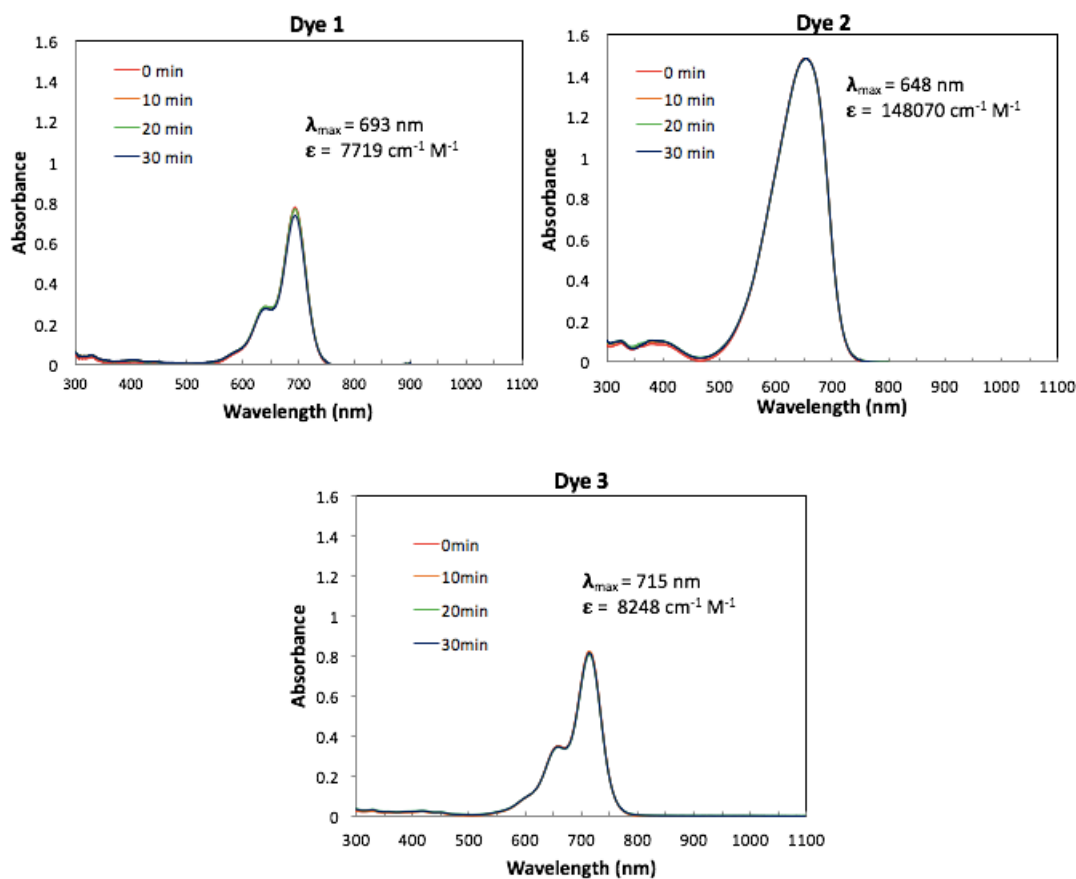


Figure 3.1 UV-visible absorption spectra of 10  $\mu\text{M}$  concentration of dyes **1**, **2**, and **3** in DMSO recorded every 10 min for 30 min in a quartz cuvette

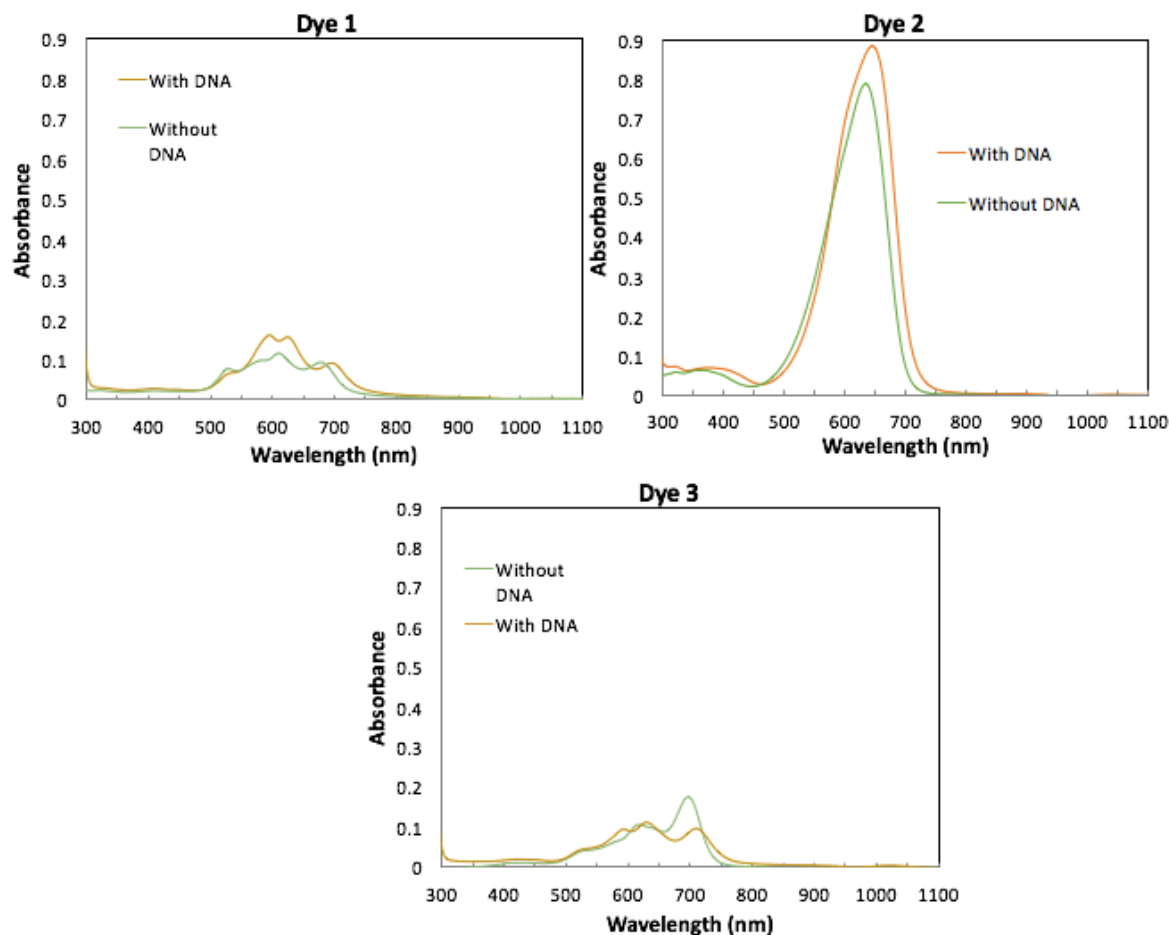


Figure 3.2 UV-Visible absorption spectra of 10  $\mu\text{M}$  dyes 1, 2, and 3 without and with 150  $\mu\text{M}$  CT-DNA in 10 mM sodium phosphate buffer pH 7.0 at  $t = 0$

It can be also seen from Figure 3.1 that the three dyes all seem to be stable at a 10  $\mu\text{M}$  concentration in DMSO, which allows us to utilize the stock solutions for a reasonable period of time before having to prepare fresh solutions from powder dye samples.

Figure 3.2 shows dye absorption in the presence and absence of DNA at  $t = 0$  in water buffered with 10 mM sodium phosphate buffer, pH 7.0. A red absorption shift was observed for each dye in the presence of DNA which is a characteristic indication of an interaction between the

dye and DNA.<sup>24</sup> Interestingly, while asymmetrical dye **2** exhibited robust absorption in DNA, absorption intensity was greatly attenuated in the aqueous buffer

Figure 3.3 shows that all three dyes exhibit a loss in absorption over time in aqueous solutions without DNA. In the presence of DNA, however, the three dyes are more stable, especially in the case of dye **1**. It is possible that this can be attributed to the bromine atom in the *meso* position of the polymethine bridge. We hypothesize that the electronegativity of this atom increases the dye stability by withdrawing electrons, slowing down the autoxidation of the dye in the aqueous solvent. The most likely dye to exhibit DNA photocleavage would therefore be expected to be dye **1**, due to its stability in the presence of DNA and resulting superior absorption in the near IR range (Figure 3.3). It is also important to note that in the presence of DNA, dyes **1** and **3** show multiple absorption maxima. Some of the peaks may be due to the presence of free and DNA-bound dye forms, vibrational fine structure, and/or aggregation of the dye in aqueous solutions either alone and/or in the presence of DNA.

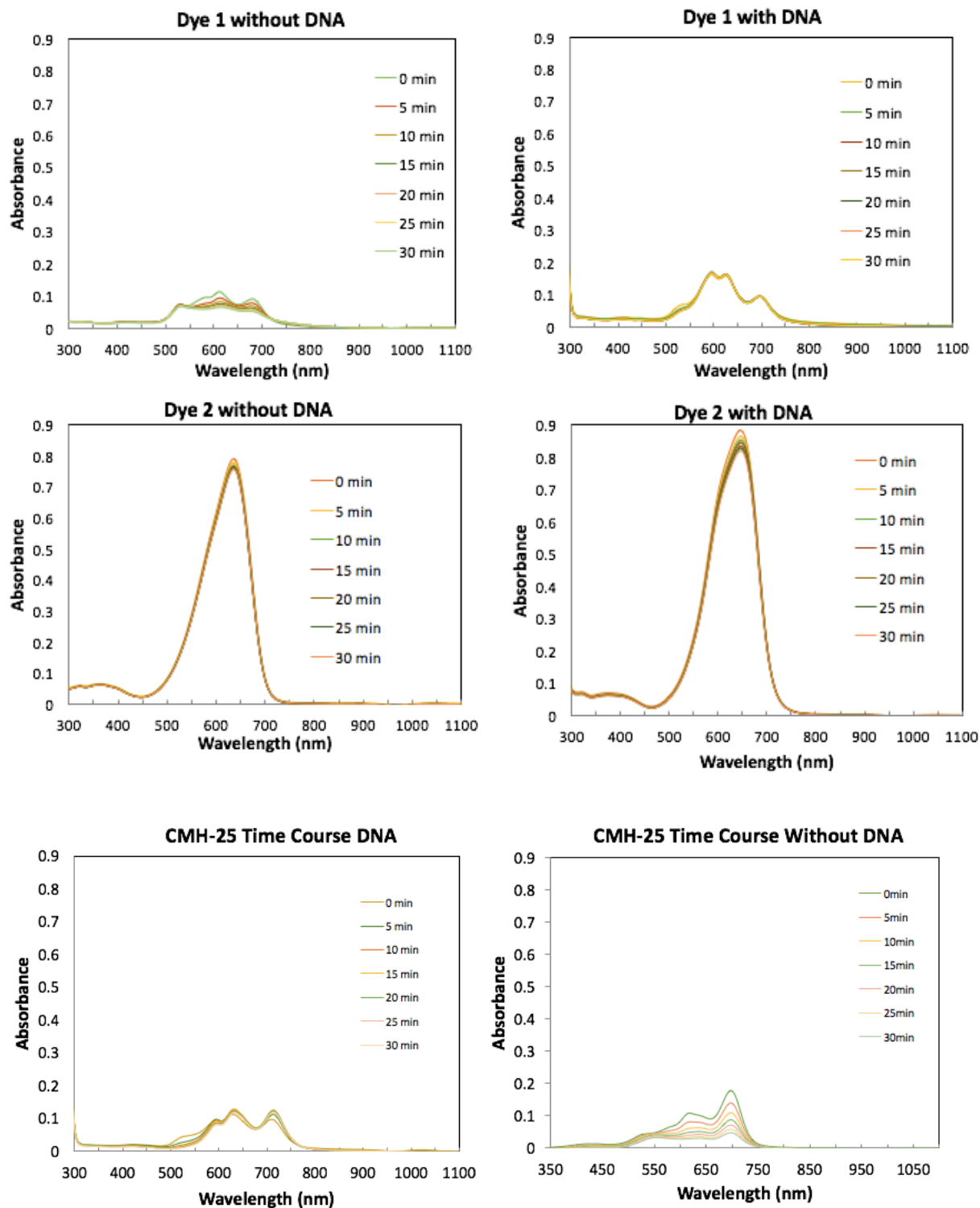


Figure 3.3 UV-Visible absorption spectra of  $10 \mu\text{M}$  dyes 1, 2, and 3 with and without  $150 \mu\text{M}$  bp of CT-DNA in  $10 \text{ mM}$  sodium phosphate buffer pH 7.0 recorded every 5 min over 30 min in a quartz cuvette.

## 3.2 Gel Electrophoresis

### 3.2.1 Determination of Optimal Light Source for Photocleavage

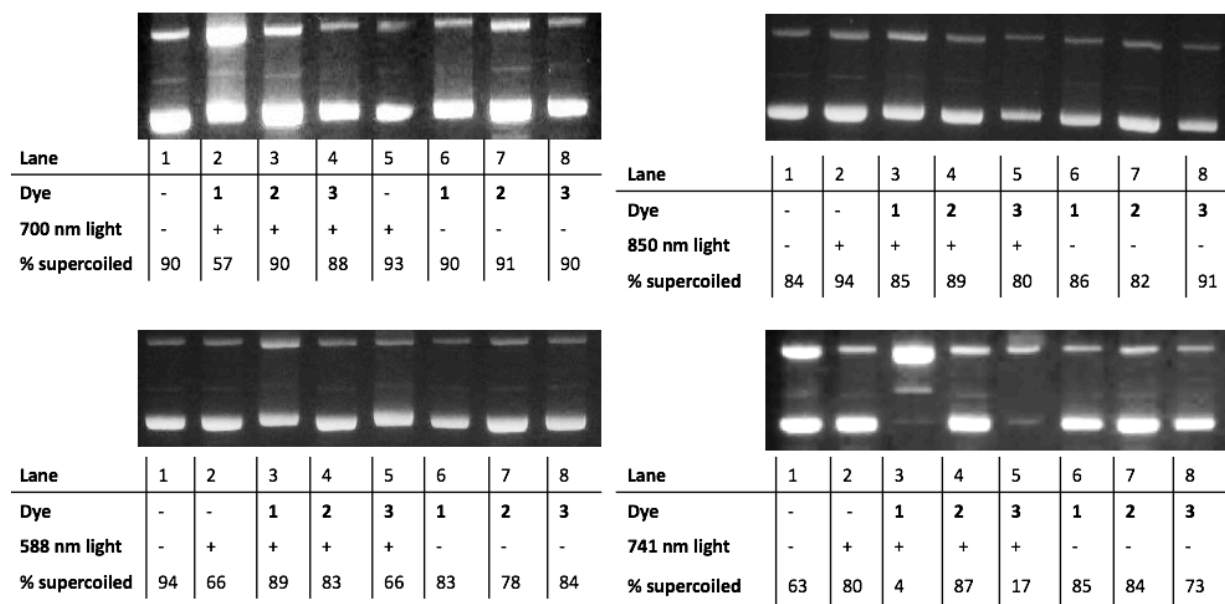


Figure 3.4 Gel electrophoresis pictures of 25  $\mu\text{M}$  dyes 1, 2, and 3 with 38  $\mu\text{M}$  b.p. of pUC19 plasmid DNA irradiated for 60 min under 700 nm (8 mW per LED), 850 nm (7.2 mW per LED), 588 nm (3 mW per LED), and 741 nm (180 mW per LED) light respectively (25  $^{\circ}\text{C}$ ).

In order to determine the best light wavelengths to use for irradiation of these dyes, multiple light sources were tested for all three dyes over an irradiation time of 1 h. The lamps used were 850 nm, 741 nm, 700 nm, and 588 nm light emitting diodes (LEDs). Gel electrophoresis was performed after irradiation of samples with these wavelengths of light. Data from these experiments provide insight into the ideal light source to use to induce ROS production from these dyes while also indicating which one of the three dyes shows the most promise as a DNA photosensitizing agent. In Figure 3.4 are photographs of electrophoresis experiments using 25  $\mu\text{M}$  of dye, 38  $\mu\text{M}$  bp of pUC19 plasmid DNA, and 10 mM sodium

phosphate buffer irradiated at 700 nm, 741 nm, 850 nm, and 588 nm for 1 h. These gels show that the best light source is the 741 nm medical lamp, which has a spectral output of 707 nm to 759 nm and has a power of 45 mW per LED. This lamp is significantly more powerful than the 700 nm, 588 nm, and 850 nm lamps which all have powers of 3 mW per LED for the 588 nm lamp, 8 mW per LED for the 700 nm lamp, and 7.2 mW per LED for the 850 nm lamp.

It is clear in Figure 3.4 that our conclusions drawn from the UV-visible experiments done are correct and that dye **1** is the most promising compound for the production of nicked DNA from supercoiled. The DNA cleavage yields are seen to be consistent with the amount of UV-visible absorption exhibited by each dye. Dye **1** exhibits the highest absorption in the presence of DNA followed by dye **3** with the lowest absorbance being seen for dye **3**. The amount of cleavage is also seen to increase with the power of each lamp used. The 741 nm lamp exhibits the highest DNA cleavage yields at 180 mW/LED of power followed by the 700 nm lamp (8 mW/LED) and 588 nm (3 mW/LED) lamp.

<b>588 nm (3 mW)</b>	$\epsilon$ ( $M^{-1}cm^{-1}$ )	% supercoiled	<b>700 (8 mW)</b>	$\epsilon$ ( $M^{-1}cm^{-1}$ )	% supercoiled
Dye <b>1</b>	9730	89	Dye <b>1</b>	9,220	57
Dye <b>2</b>	55,800	83	Dye <b>2</b>	24,700	90
Dye <b>3</b>	8,930	66	Dye <b>3</b>	8,660	88
<b>741 nm (180 mW)</b>	$\epsilon$ ( $M^{-1}cm^{-1}$ )	% supercoiled	<b>850 nm (7.2 mW)</b>	$\epsilon$ ( $M^{-1}cm^{-1}$ )	% supercoiled
Dye <b>1</b>	1,580	4	Dye <b>1</b>	390	85
Dye <b>2</b>	2,400	87	Dye <b>2</b>	150	89
Dye <b>3</b>	9,950	17	Dye <b>3</b>	540	80

*Table 3.1 Molar extinction coefficients and cleavage yields reported as % supercoiled DNA for dyes **1**, **2**, and **3** with lamps at 588 nm, 700 nm, 741 nm, and 850 nm.*

The results from this experiment (Figure 3.4) show near quantitative cleavage of supercoiled pUC19 plasmid with dye **1** and dye **3**. The 741 nm lamp produced the highest yields

of cleavage compared to the 700 nm and 588 nm lamps. These three lamps all emit light in the absorbance wavelength of dyes **1**, **2**, and **3**. Table 3.1 shows a comparison of the molar extinction coefficients of each dye at the irradiation wavelength of the lamps. While dyes **1** had the highest molar extinction coefficient at 588 nm this lamp also had the lowest power of the three. Dye **3** had the highest molar extinction coefficient at 741, which also produced the highest cleavage. All dyes had low absorbance at 850 nm and therefore a low molar extinction coefficient. This lamp was used as a dark control.

To ensure that the observed cleavage was produced due to a photochemical reaction and not a thermal reaction, temperature controls were added and samples of dyes **1**, **2**, and **3**, were irradiated in a metal block in an ice bath and the temperature monitored using a thermometer inserted into the metal block (Figure 3.5).

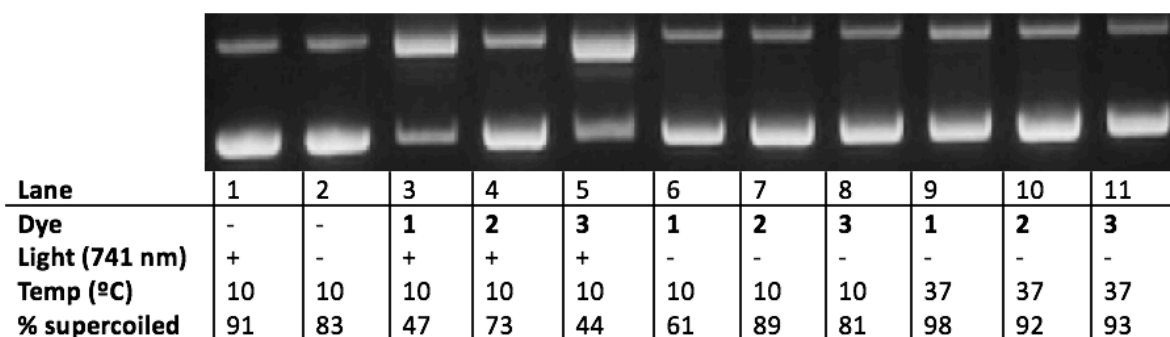


*Figure 3.5 Temperature controlled gel electrophoresis experiment with 25  $\mu$ M of dyes **1**, **2**, and **3**, with 38  $\mu$ M bp of DNA, 10 mM of sodium phosphate buffer pH 7.0 at 10 °C with dark controls at 10 °C and 37°C irradiated at 741 nm with 180 mW of power for 1 h.*

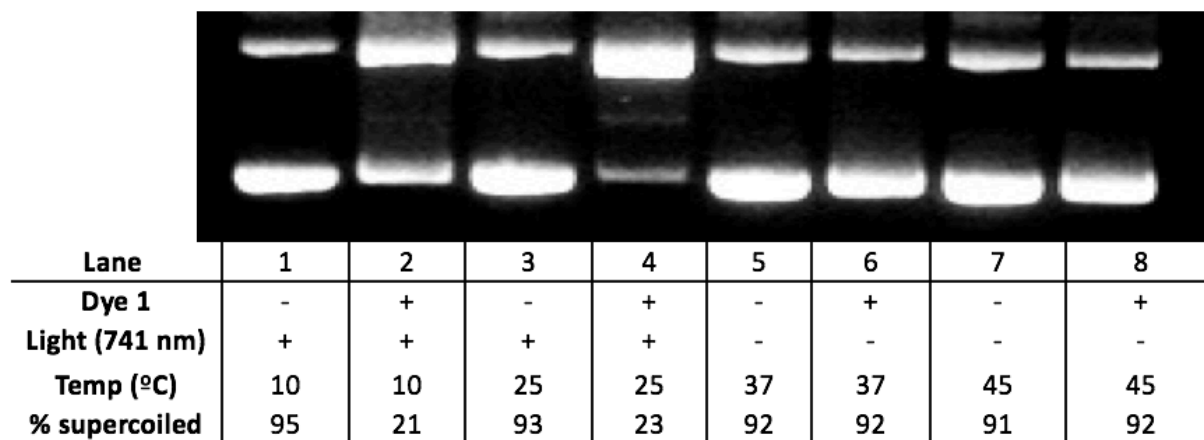


*Figure 3.6 Gel electrophoresis experiment of dye 1 at 25  $\mu\text{M}$  concentrations in the presence of 38  $\mu\text{M}$  bp DNA and 10 mM sodium phosphate buffer pH 7.0 with dark controls at 45  $^{\circ}\text{C}$  and 37  $^{\circ}\text{C}$  to ensure that cleavage observed is due to the presence of light and not heat*

The temperature controlled experiments reveal minimal amounts of nicked DNA in the absence of light. In Figure 3.5, the intensity of the nicked bands remains relatively constant from the light control lane 1 and the reactions in the dark at 10  $^{\circ}\text{C}$  and 37  $^{\circ}\text{C}$ , showing that heat does not appear to generate a major increase the yields of DNA cleavage.

Although it seems that dye **3** is able to cleave supercoiled DNA, its UV-Visible spectra reveal that this compound is very unstable in an aqueous environment (Figure 3.3). This factor likely makes dye **3** unusable for PDT treatment. It is possible that the enhanced photocleavage of dye **1** compared to its two analogs may be supported by the heavy atom effect. The bromine substituent can induce this effect by increasing the rate of intersystem crossing to the spin-forbidden triplet state.<sup>25, 26</sup> The enhanced photocleavage may also be explained by the fact that dye **1** is more stable than dyes **2** and **3** when DNA is present. The temperature control experiment was then repeated again for dye **1** with increased temperature for the dark controls to ensure that the high cleavage produced from this dye was a product of a photochemical reaction and not a thermal reaction. Figure 3.6 shows again that heat does not increase the amount of DNA cleavage produced

from dye **1** in photocleavage reactions, but not in dark control reactions in which compound **1** is present.

### 3.2.2 Concentration Titrations

Knowing that symmetrical quinoline dye **1** has superior stability and high cleavage yields at a 25  $\mu\text{M}$  concentration, it was important to further explore the potential of this compound as a DNA photosensitizing agent. Optimizing the concentration of dye per sample ensures that there is minimal waste and maximum ROS production for efficient cleavage results. Samples were irradiated at 741 nm for 1h with varying amounts of dye **1** ranging in concentration from 0  $\mu\text{M}$ , as a control, to 48  $\mu\text{M}$ .

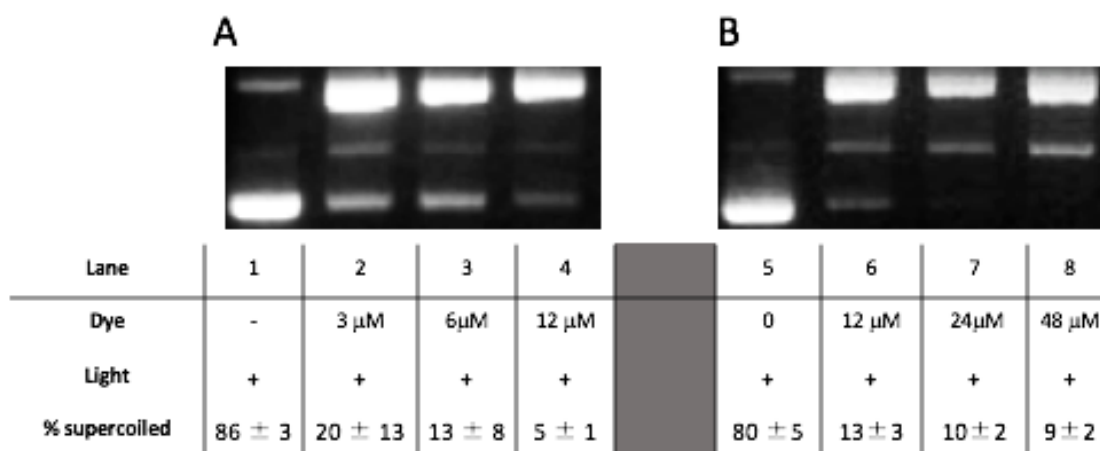


*Figure 3.7 Concentration titration gel electrophoresis experiments of dye **1** at varying concentrations with 38  $\mu\text{M}$  bp pUC19 plasmid DNA, 10 mM sodium phosphate buffer, pH 7.0, irradiated at 741 nm with a 180 mW LED lamp for 60 min at 10  $^{\circ}\text{C}$ .*

Figure 3.7 shows that even at 12  $\mu\text{M}$  concentration, dye **1** was able to cleave DNA in very high yields. At 24  $\mu\text{M}$  of dye **1**, cleavage appears to be near completion with only a very faint

supercoiled band able to be seen in lane 7. These experiments were done in triplicate (Figure 0.1 and Figure 0.2). All future reactions with this dye were therefore done at a 24  $\mu\text{M}$  concentration.

### 3.2.3 *Reaction Kinetics*

In order to determine the kinetics for the reaction between dye **1**, DNA, and light, it was necessary to know how quickly the reaction reached completion. A plot of concentration vs. time would give insight into the reaction rate. For these experiments, a large 250  $\mu\text{L}$  sample of 24  $\mu\text{M}$  dye **1** was irradiated through the side of a plastic cuvette with the 741 nm lamp in the presence of 38  $\mu\text{M}$  bp pUC19 plasmid DNA and 100 mM sodium phosphate buffer, pH 7.0 at 25  $^{\circ}\text{C}$ . Aliquots removed at time points of 5 min, 10 min, 30 min, 60 min, 80 min, and 100 min show the progression of supercoiled into nicked and linear forms of pUC19 (Figure 3.8). Reactions were completed in triplicate (Figure 0.3 and Figure 0.4). Cleavage increased steadily from 0 min until 80 min. This gel in Figure 3.8 is consistent with the appearance of the reactions removed from the cuvette after irradiation losing color until finally, at 60 min, the sample was colorless.

This phenomenon in which the color fades during these photocleavage reactions is a limiting factor known as photobleaching, or photooxidation. This is a decomposition of molecules due to oxidation from the ROS produced by the spin-forbidden transition of a molecule's energy from an excited singlet state to the triplet state.<sup>2</sup> The decomposition of the dye molecule would appear as a loss of color over time. The tolerance towards photooxidation varies between molecules with pentamethine cyanine dyes having higher other polymethine chain lengths.<sup>27</sup>

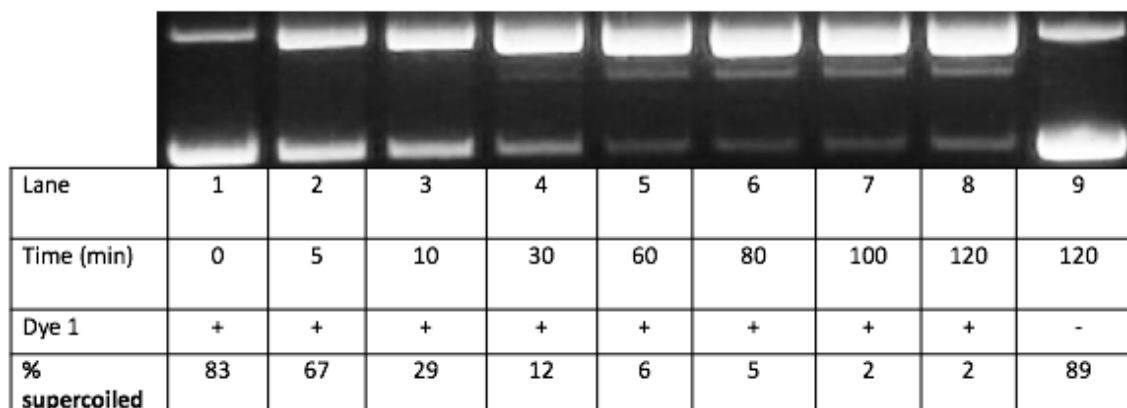


*Figure 3.8 Gel picture of 24  $\mu\text{M}$  dye 1 in the presence of 38  $\mu\text{M}$  bp pUC19 plasmid DNA and 10 mM sodium phosphate buffer, pH 7.0, over time at 25  $^{\circ}\text{C}$*

Upon triplication of this experiment it was possible to determine the reaction order for the photo-conversion of supercoiled DNA to cleaved DNA by calculating the percentage of supercoiled vs cleaved in each lane. Figure 3.10 shows that a plot of  $1/ [\% \text{ supercoiled}]$  v. time yields a straight line which is consistent with a second order reaction. The rate constant,  $k$ , for the second order reaction is equal to the slope of the line. Averaged over three trials,  $k$  for dye 1 is  $.002 \text{ M}^{-1}\text{sec}^{-1}$  with a standard deviation of  $1.30 \times 10^{-3}$ . The remaining two graphs can be found in the appendix (Figure 0.5).

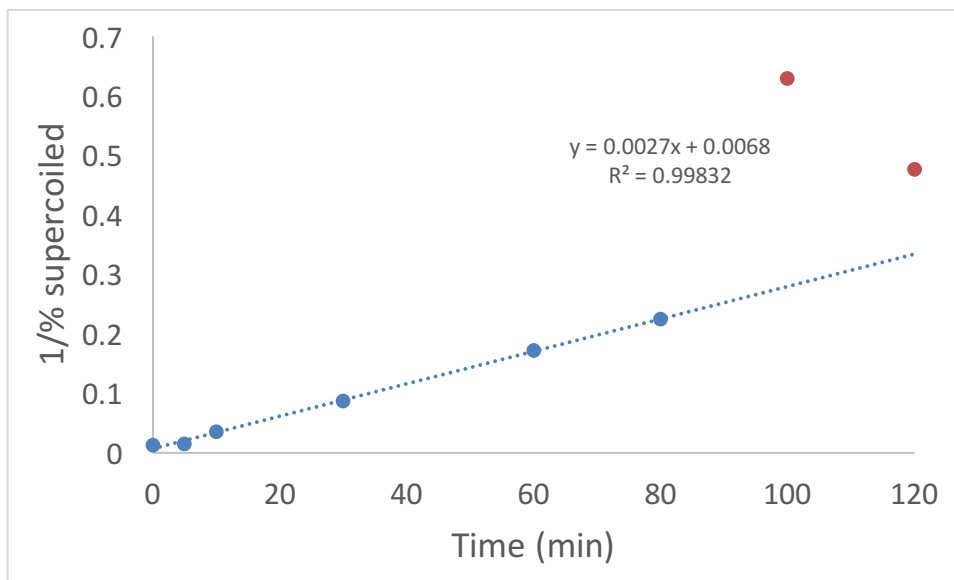


*Figure 3.9 reciprocal plot of concentration v. time showing the reaction order to be second order for 24  $\mu\text{M}$  of dye with 38  $\mu\text{M}$  bp DNA and 10 mM sodium phosphate buffer pH 7.0. Data points in red were excluded from the curve fitting procedure*

### 3.2.4 ROS Scavengers

Reagents were added to photocleavage experiments to observe the resulting change in pUC19 photocleavage. Several reagents were chosen for their ability to scavenge specific ROS. Sodium azide was selected for its ability to quench singlet oxygen. To verify that the results from the sodium azide experiment were due to  $^1\text{O}_2$ , photocleavage experiments were repeated with  $\text{D}_2\text{O}$  as a replacement for water. The presence of  $\text{D}_2\text{O}$  should increase the lifetime of  $^1\text{O}_2$  leading to an enhancement in photocleavage compared to samples with water. Additional photocleavage experiments were performed with EDTA, a known metal chelator that should decrease the cleavage by chelating trace levels of redox active metal cations in solution. Sodium benzoate, a known hydroxyl radical scavenger, was used in samples to test for the involvement of  $\bullet\text{OH}$  in the photocleavage reactions. If  $\bullet\text{OH}$  were being generated, it would be likely for the compound to have undergone a type I electron transfer, reducing ground state triplet oxygen to superoxide anion

radical ( $O_2^{\cdot-}$ ). Superoxide would then react to form hydrogen peroxide (Figure 1.5). To prove this, catalase was added to samples to convert any  $H_2O_2$  to  $H_2O$ . If  $H_2O_2$  were contributing to photocleavage, then a decrease in cleavage would be observed upon catalase addition.

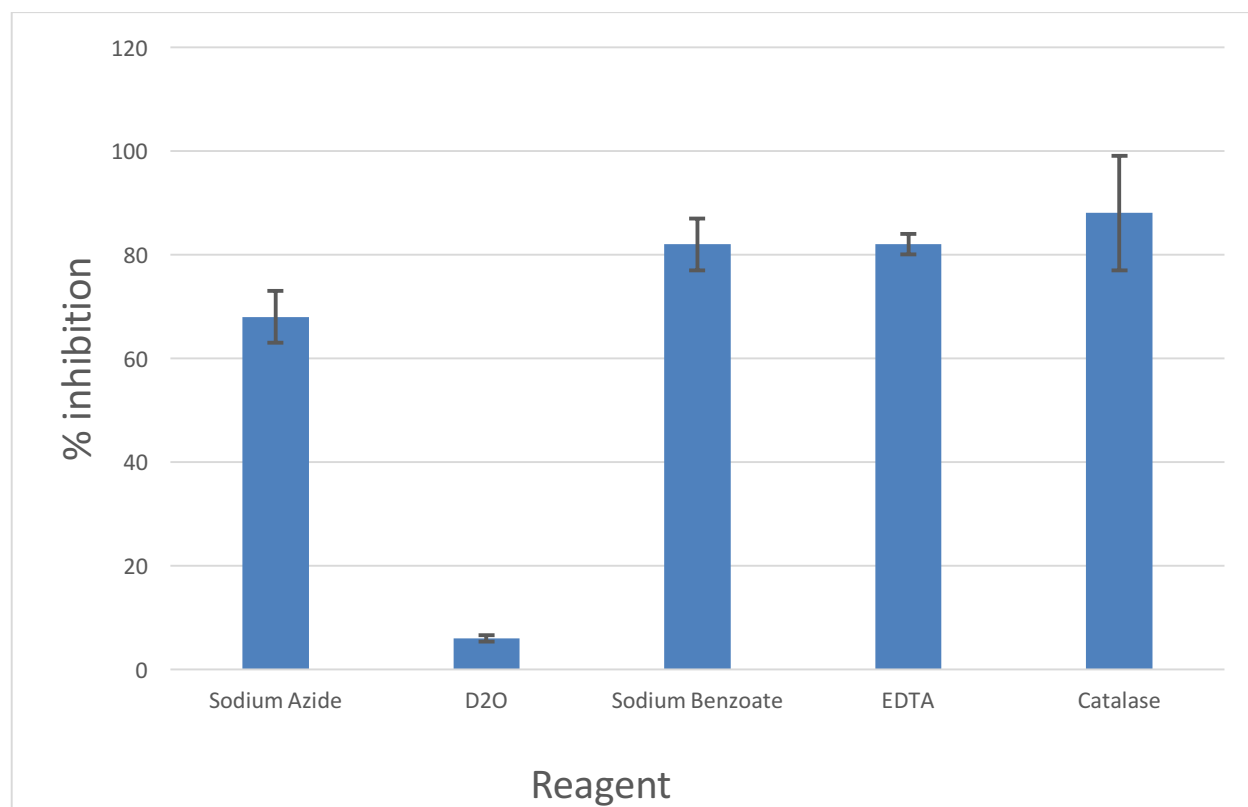


*Figure 3.10 Comparison of % inhibition of photocleavage by added chemical agents. Error over three trials is reported as standard deviation.*

The percent photocleavage inhibition data shown in Figure 3.10 suggests that dye **1** undergoes a type I electron transfer reaction from the excited triplet state to ground state oxygen resulting in the ultimate production of DNA damaging  $\cdot OH$  in the photocleavage reactions with this compound. The high yield of inhibition caused by the introduction of sodium benzoate and catalase indicates the respective participation of  $\cdot OH$  and  $H_2O_2$  in DNA photocleavage. The high inhibition from the addition of sodium azide might be due to a side reaction with hydroxyl radicals, a hypothesis that is supported by the inhibition, not enhancement, of photocleavage by the

substitution of D<sub>2</sub>O for H<sub>2</sub>O. The metal chelating agent EDTA strongly inhibited photocleavage pointing to the involvement of redox active metal ions. Taken together, the data suggest that DNA photocleavage might be occurring by Fenton chemistry as shown in Figure 1.5. The involvement of singlet oxygen in the photocleavage reactions is not supported by our experiments. Triplicated photocleavage gel pictures can be found in the appendix (Figures 0.6 - 0.10).

These hydroxyl radicals are powerful oxidizing reagents that are able to cause damage to many biological tissues such as DNA, lipids, and proteins.<sup>15</sup> With a diffusion distance of only 20 these radicals are likely to interact with DNA when produced by a ligand. This interaction results in the loss of hydrogen atoms from the deoxyribose sugar.<sup>28</sup>

### **3.3 Binding Mode Investigation**

There are many ways that dye **1** would be able to interact with DNA that would allow it to be in close enough proximity for the ROS production from irradiation of the dye to cause damage. The diffusion rate of hydroxyl radicals is  $\sim 20 \text{ \AA}$ , so the reaction must proceed while the dye is directly adjacent to DNA for damage to occur.<sup>29</sup> Circular dichroism spectra were recorded in order to give insight with respect to the achiral dye molecule binding to the chiral DNA molecule through intercalation, groove binding, or both.

#### **3.3.1 UV-Visible Absorption Saturation**

In order to acquire induced CD spectra, it was important to know the concentration of CT-DNA that would be needed to completely bind dye **1**. To do this, absorption spectra were recorded in which 10  $\mu\text{M}$  of dye was added to a cuvette with 10 mM sodium phosphate buffer, pH 7.0, and ddH<sub>2</sub>O to make the total sample volume 500  $\mu\text{L}$ . By adding small increments of CT-DNA to the cuvette, the absorption changed until the titration endpoint was reached. The concentration of DNA used to reach this point would then be used in CD experiments, ensuring that the spectra captured

a fully bound dye-DNA complex. Figure 3.11 shows that the blue shifted and center absorption bands are both unchanging at 646.23  $\mu\text{M}$  bp of CT-DNA. The red shifted band, on the other hand, never seemed to truly reach saturation.

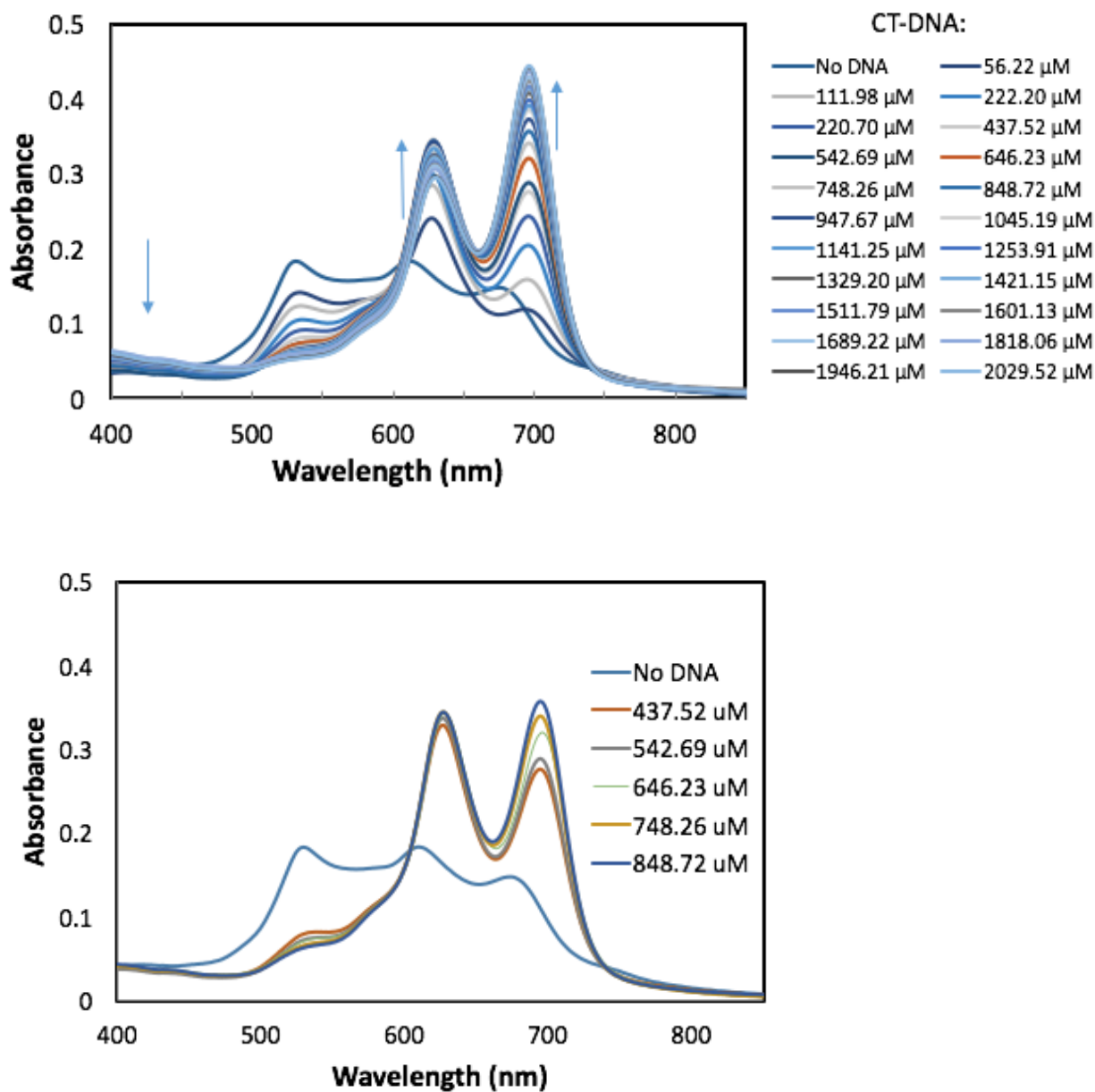


Figure 3.11 UV-Visible absorption titration of 10  $\mu\text{M}$  dye 1 and increasing concentrations of CT-DNA in 10 mM sodium phosphate buffer, pH 7.0

### 3.3.2 *Circular Dichroism*

Using the 646.23  $\mu\text{M}$  bp concentration of DNA, CD spectra were recorded for 10  $\mu\text{M}$  of dye **1**, DNA, and 10 mM sodium phosphate buffer, pH 7.0, from 800 nm to 200 nm. Because of the high concentration of DNA, the characteristic DNA signal at  $\sim 260$  nm is very large making it necessary to view the spectra at two different scales. Figure 3.12 shows a strong bisignate ICD peak of the dye-DNA complex followed by a positive peak. This combination suggests polymeric groove binding of the dye to DNA.<sup>11, 30</sup> Figure 3.13 shows an attenuation of the DNA CD signal at 280 nm once dye **1** is introduced. This suggests that the DNA is being unwound by the dye either through an intercalative or groove binding mode.<sup>30, 31</sup>

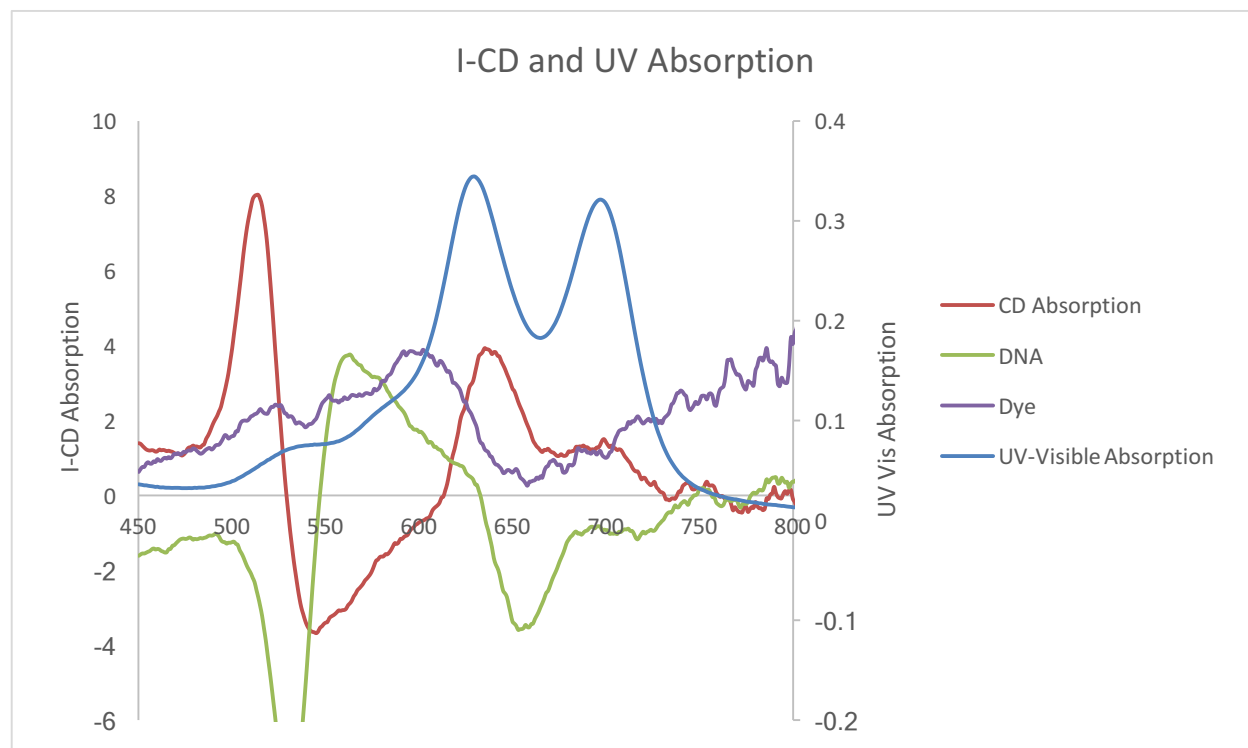
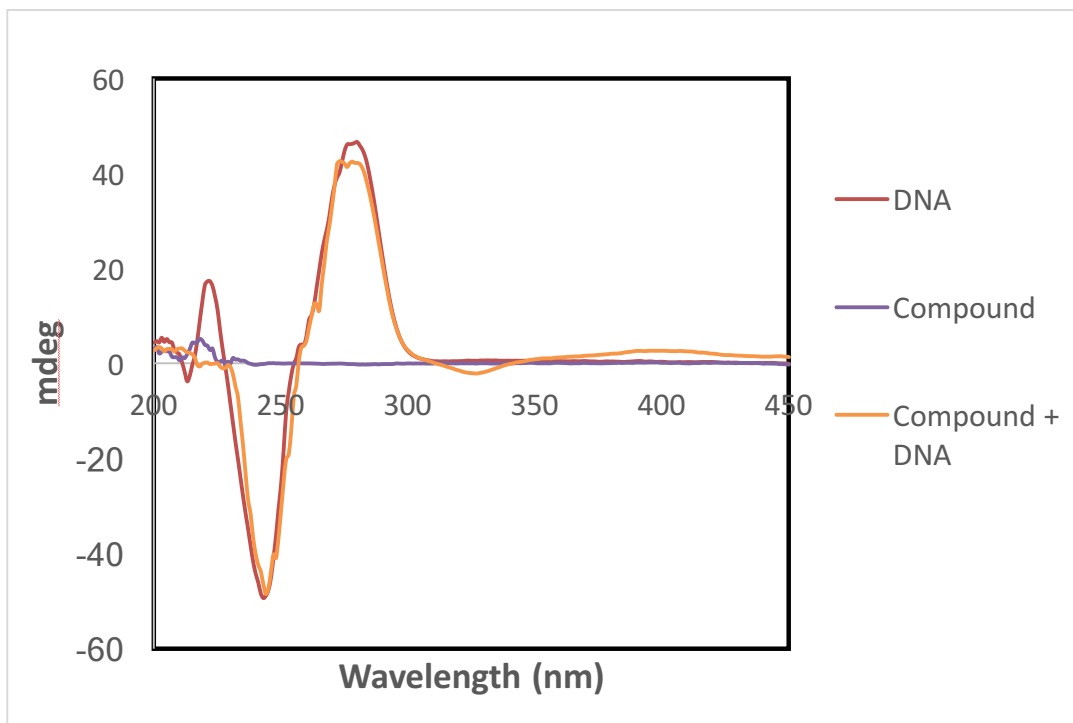


Figure 3.12 UV-visible and CD spectra of 10  $\mu\text{M}$  dye **1** with 646.23  $\mu\text{M}$  bp of CT-DNA in 10 mM sodium phosphate buffer pH 7.0



*Figure 3.13 CD absorption spectra of 10  $\mu\text{M}$  dye 1, 646.23  $\mu\text{M}$  bp CT DNA, 10 mM sodium phosphate buffer, pH 7.0, from 450 to 200 showing the DNA unwinding upon the binding to dye 1*

By overlap of the induced CD spectrum with the UV-visible spectrum (Figure 3.12) of the dye in the presence of DNA, it is possible to see the correlation between the two. The midpoint of the induced bisignate band is in the same location as an absorbance maximum, while the two positive ICD signals are aligned exactly with absorption peaks produced the dye-DNA complex. Typically, molecules that interact with DNA via intercalation must be small in order to fit between the base pairs. The induced CD signals exhibited by intercalation are therefore much weaker than the groove binding molecule that takes up much more space on the DNA. This knowledge strengthens the evidence of groove binding from the CD spectra. A molecule that exhibits higher ordered aggregates would be too large to effectively intercalate. Moreover, the ICD signals are strong rather than weak, again pointing to groove binding.

### 3.3.3 UV-Visible Absorption Changes Induced by Pentamidine and Ethidium Bromide

#### *Addition*

In order to verify that dye **1** binds to DNA as a groove binder, UV-visible spectra were recorded for the dye without DNA, with DNA, and with DNA pre-equilibrated for 1 min with pentamidine, a known minor groove binder, or, pre-equilibrated DNA with ethidium bromide, a known intercalator. Figure 3.14 shows that with the pre-equilibration of DNA and pentamidine, there is a decrease in the absorption of the dye DNA complex. Combined with the CD results, it can be assumed that this decrease is a result from the pentamidine blocking the dye from binding to the minor groove.

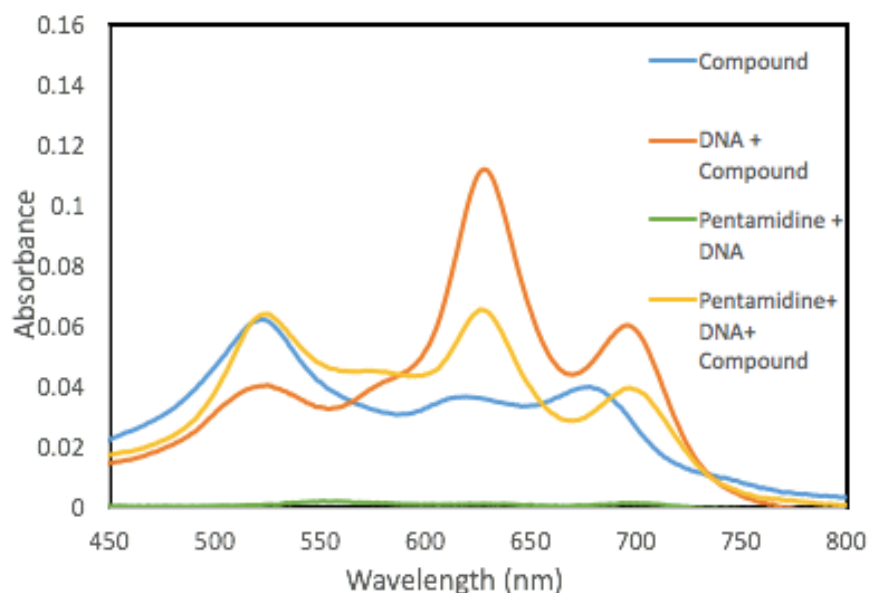


*Figure 3.14 UV-visible absorbance spectra to observe the effects of addition of 10  $\mu$ M pentamidine to a solution of 10  $\mu$ M dye **1** with 150  $\mu$ M bp CT-DNA and 10 mM sodium phosphate buffer*

Repeating this experiment with ethidium bromide shows that there is an increase in absorption upon pre-equilibration with EtBr for 1 min (Figure 3.15). Other than that change, the shape of

the peaks remains the same. Thus, the release of free compound **1** upon EtBr binding is not indicated.

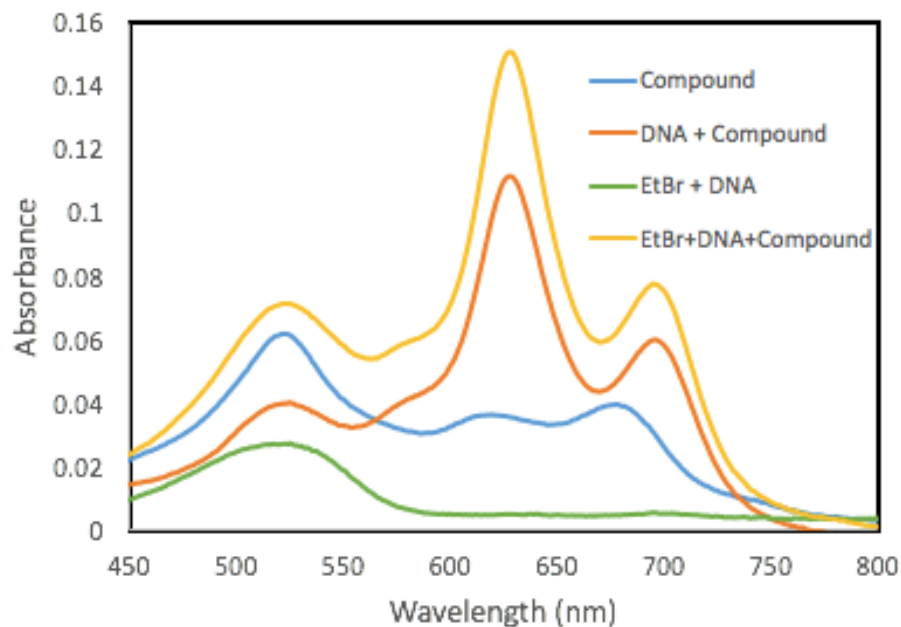


*Figure 3.15 UV-visible spectra of EtBr with DNA to observe the effects of the addition of 10  $\mu\text{M}$  EtBr to DNA on dye **1***

The binding constants of pentamidine and EtBr to CT-DNA are  $6.07 \times 10^5 \text{ M}^{-1} \text{ sec}^{-1}$  and  $1.0 \times 10^7 \text{ M}^{-1} \text{ sec}^{-1}$  explaining that EtBr binds more tightly to CT-DNA than pentamidine.<sup>32, 33</sup> Because the dye was undeterred from binding to the DNA-EtBr complex but not able to bind to the weaker-bound DNA-pentamidine complex, we conclude that dye **1** binds to DNA in the minor groove.

## 4 CONCLUSIONS

The investigation of novel cyanine dyes for use as photosensitizers for photodynamic therapy is necessary because of the lack of suitable PS clinically available for use globally. Their high molar extinction coefficient makes them ideal candidates for producers of the damaging ROS. The ability to easily synthesize these dyes with near-IR absorption gives these compounds an advantage to currently used PS for PDT. This research focuses on the characterization of cyanine dyes with structural similarities to determine the most effective properties towards increased photocleavage yields.

UV-visible absorption spectra highlight the significance on the addition of an electronegative atom in the *meso* position of the dye. The most stable of the three compounds was dye **1**, a symmetrical quinoline pentamethine cyanine dye with a bromine atom in the *meso* position. Dye **1** has a molar extinction coefficient of  $11460 \text{ L mol}^{-1} \text{ cm}^{-1}$ . When bound to DNA, the dye absorbs light from 480 nm to 900 nm with absorption maxima at 534 nm, 596 nm, 627 nm, and 698 nm. Compared with the proton substituted compounds **2**, an asymmetrical cyanine dye with a quinoline ring and an indole ring, and **3**, a symmetrical proton substituted quinoline cyanine, the stability over time of compound **1** was the highest both with and without CT-DNA. Dye **1** and **3** were also noticed to have either various aggregation states or vibrational fine structure which were evident by the three peaks in the UV-visible spectra for those compounds.

Different lamps were tested to determine the ideal light source to use for irradiation. This was done in part, also, to gain perspective on which dyes would show cleavage of supercoiled pUC19 to its nicked and linear forms. Out of the four lamps tested, 588 nm, 700 nm, 741 nm, and 850 nm, the 741 nm lamp produced optimal cleavage results for dye **1** and **3**. This was counterintuitive at first, because of the minimal absorption seen from these dyes at 741 nm but,

the 741 nm lamp used has much higher power than the other lamps and a spectral output of 707-759 nm. The decision was made to do further experiments only with dye **1** due to dye **3**'s relatively unstable nature in the presence of DNA.

Once a light source was selected, dye concentration and DNA photocleavage irradiation time were optimized with gel electrophoresis experiments. Dye **1** was seen to have the highest cleavage of supercoiled plasmid at 24  $\mu\text{M}$  but it is interesting to note that this compound also had very high cleavage yields at lower micromolar concentrations. At 24  $\mu\text{M}$ , the ideal irradiation time was found to be approximately 60 min. By plotting a graph of  $1/[\% \text{supercoiled}]$  v. time, a second order kinetics equation was achieved and the rate constant at 25  $^{\circ}\text{C}$  found to be  $k = 0.002 \text{ M}^{-1} \text{ s}^{-1}$  with a standard deviation of  $1.30 \times 10^{-3}$  over three trials. It was also determined, through scavenger experiments, that dye **1** undergoes a type I electron transfer from its excited triplet state to ground state molecular oxygen. This resulted in the production of  $\text{H}_2\text{O}_2$  and then DNA damaging  $\bullet\text{OH}$  by Fenton chemistry.

To study how dye **1** binds to DNA, circular dichroism experiments were performed to see if any signature peaks were observable. The bisignate peak of induced CD at the same wavelength of the absorbance spectrum suggests that a higher ordered aggregate of the compound is binding to the DNA minor groove. The data from CD paired with the UV spectra showing that dye **1** is blocked from binding to DNA by a known minor groove binder point strongly to the conclusion that dye **1** binds to DNA through the minor groove.

Studying these cyanine dyes as photosensitizers is useful for many reasons, but their absorption in the near IR gives them an advantage over a lot of compounds, even those currently being used for PDT. The differences in results between dyes **1**, **2**, and **3** spectroscopically and with photocleavage show that structure has a role to play in these dyes' efficiency with the most

active compound possessing two symmetrical quinoline ring systems with an electronegative substituent at the *meso* position of the polymethine bridge linking the two rings. The bromine is likely to stabilize the molecule from autoxidation and may even introduce a heavy atom effect. Both of these phenomena may lead to increased photocleavage. The indole ring in dye **2** decreases the stability of the compound in buffered water compared with the two six-membered components of quinoline.

The ability to treat many forms of cancer with minimal side effects would be a significant gain in the success of biomedical research. Reaching this goal is the aim of many researchers and begins with the discovery of compounds that will damage targeted tumors and little else. Photodynamic therapy is already making waves as a promising treatment for superficial tumors and lesions. The discovery of diverse photosensitizers that have applications in many areas of the body will pave the way for more innovation. Cyanines have great potential because of their efficiency at producing DNA damaging ROS, low toxicity, and the ability to strongly absorb deeply penetrating light in the near infrared wavelength range.

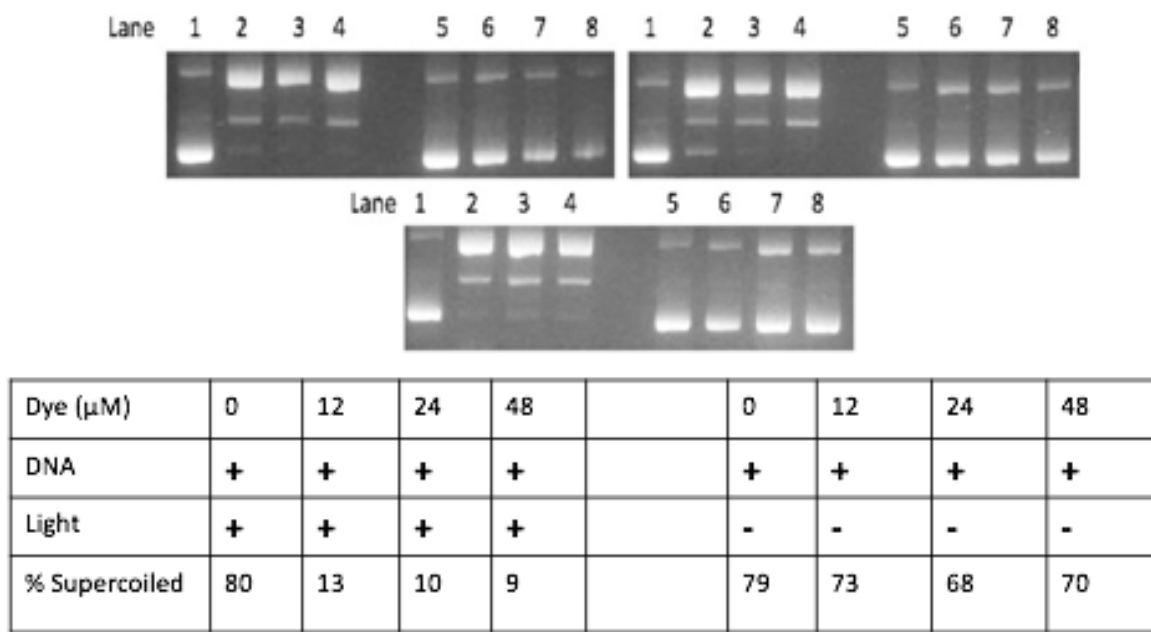
## REFERENCES

1. E. J. Van Lare, *Kirk-Othmer Encycl. Chem. Technol.*, 2nd Ed., 1965, **6**, 605-624.
2. B. Jedrzejewska, A. Bajorek and J. Moraczewska, *Appl. Spectrosc.*, 2013, **67**, 672-680.
3. J. Klohs, A. Wunder and K. Licha, *Basic Research In Cardiology*, 2008, **103**, 144-151.
4. B. A. Armitage, *Top. Curr. Chem.*, 2005, **253**, 55-76.
5. S. Pascal, A. Haefele, C. Monnereau, A. Charaf-Eddin, D. Jacquemin, B. Le Guennic, O. Maury and C. Andraud, 2014.
6. M. Henary and M. Mojzych, *Top. Heterocycl. Chem.*, 2008, **14**, 221-238.
7. G. Beckford, E. Owens, M. Henary and G. Patonay, *Talanta*, 2012, **92**, 45-52.
8. J. S. Kim, R. Kodagahally, L. Strekowski and G. Patonay, *Talanta*, 2005, **67**, 947-954.
9. D. Saccone, S. Galliano, N. Barbero, P. Quagliotto, G. Viscardi and C. Barolo, *Eur. J. Org. Chem.*, 2016, **2016**, 2244-2259.
10. T. Biver, A. Boggioni, F. Secco, E. Turriani, M. Venturini and S. Yarmoluk, *Arch. Biochem. Biophys.*, 2007, **465**, 90-100.
11. J. L. Seifert, R. E. Connor, S. A. Kushon, M. Wang and B. A. Armitage, *J. Am. Chem. Soc.*, 1999, **121**, 2987-2995.
12. P. Agostinis, K. Berg, K. A. Cengel, T. H. Foster, A. W. Girotti, S. O. Gollnick, S. M. Hahn, M. R. Hamblin, A. Juzeniene, D. Kessel, M. Korbelik, J. Moan, P. Mroz, D. Nowis, J. Piette, B. C. Wilson and J. Golab, *CA Cancer J Clin*, 2011, **61**, 250-281.
13. E. Delaey, F. Van Laar, D. De Vos, A. Kamuhabwa, P. Jacobs and P. De Witte, *J. Photochem. Photobiol., B*, 2000, **55**, 27-36.
14. D. Trachootham, J. Alexandre and P. Huang, *Nat. Rev. Drug Discovery*, 2009, **8**, 579-591.
15. Z. Li and K. B. Grant, *RSC Advances*, 2016, **6**, 24617-24634.
16. S. Enami, Y. Sakamoto and A. J. Colussi, *Proc. Natl. Acad. Sci. U. S. A.*, 2014, **111**, 623-628.
17. A. M. Smith, M. C. Mancini and S. Nie, *Nat. Nanotechnol.*, 2009, **4**, 710-711.
18. R. R. Allison, G. H. Downie, R. Cuenca, X.-H. Hu, C. J. H. Childs and C. H. Sibata, *Photodiagn. Photodyn. Ther.*, 2004, **1**, 27-42.
19. Z. Zhou, J. Song, L. Nie and X. Chen, *Chemical Society Reviews*, 2016, **45**, 6597-6626.
20. A. P. Castano, T. N. Demidova and M. R. Hamblin, *Photodiagnosis and photodynamic therapy*, 2004, **1**, 279-293.
21. B. C. Wilson and M. S. Patterson, *Phys. Med. Biol.*, 2008, **53**, R61-R109.
22. A. R. Montazerabadi, A. Sazgarnia, M. H. Bahreyni-Toosi, A. Ahmadi and A. Aledavood, *Journal of Photochemistry and Photobiology B: Biology*, 2012, **109**, 42-49.
23. J. Atchison, S. Kamila, H. Nesbitt, K. A. Logan, D. M. Nicholas, C. Fowley, J. Davis, B. Callan, A. P. McHale and J. F. Callan, *Chemical Communications*, 2017, **53**, 2009-2012.
24. A. L. Mikheikin, A. L. Zhuze and A. S. Zasedatelev, *J. Biomol. Struct. Dyn.*, 2000, **18**, 59-72.
25. A. Gorman, J. Killoran, C. O'Shea, T. Kenna, W. M. Gallagher and D. F. O'Shea, *J. Am. Chem. Soc.*, 2004, **126**, 10619-10631.
26. S. E. Braslavsky, A. U. Acuna, W. Adam, F. Amat, D. Armesto, T. D. Z. Atvars, A. Bard, E. Bill, L. O. Bjoern, C. Bohne, J. Bolton, R. Bonneau, H. Bouas-Laurent, A. M. Braun, R. Dale, K. Dill, D. Doepp, H. Duerr, M. A. Fox, T. Gandolfi, Z. R. Grabowski, A. Griesbeck, A. Kutateladze, M. Litter, J. Lorimer, J. Mattay, J. Michl, R. J. D. Miller,

- L. Moggi, S. Monti, S. Nonell, P. Ogilby, G. Olbrich, E. Oliveros, M. Olivucci, G. Orellana, V. Prokorenko, K. R. Naqvi, W. Rettig, A. Rizzi, R. A. Rossi, E. San Roman, F. Scandola, S. Schneider, E. W. Thulstrup, B. Valeur, J. Verhoeven, J. Warman, R. Weiss, J. Wirz and K. Zachariasse, *Pure Appl. Chem.*, 2007, **79**, 293-465.
27. A. P. Gorka and M. J. Schnermann, *Current Opinion in Chemical Biology*, 2016, **33**, 117-125.
28. B. Balasubramanian, W. K. Pogozelski and T. D. Tullius, *Proc. Natl. Acad. Sci. U. S. A.*, 1998, **95**, 9738-9743.
29. D. E. Williams, C. M. Fischer, M. Kassai, L. Gude, M.-J. Fernández, A. Lorente and K. B. Grant, *Journal of Inorganic Biochemistry*, 2017, **168**, 55-66.
30. N. C. Garbett, P. A. Ragazzon and J. B. Chaires, *Nat. Protoc.*, 2007, **2**, 3166-3172.
31. Y.-C. Zheng, M.-L. Zheng, Z.-S. Zhao and X.-M. Duan, *Proc. SPIE*, 2014, **8947**, 894722/894721-894722/894727.
32. E. Sundaravadivel, S. Vedavalli, M. Kandaswamy, B. Varghese and P. Madankumar, *RSC Advances*, 2014, **4**, 40763-40775.
33. A. Kellett, M. O'Connor, M. McCann, M. McNamara, P. Lynch, G. Rosair, V. McKee, B. Creaven, M. Walsh, S. McClean, A. Foltyn, D. O'Shea, O. Howe and M. Devereux, *Dalton Transactions*, 2011, **40**, 1024-1027.

## APPENDICES

## Appendix A

*Appendix A.1*

*Figure 0.1 Gel electrophoresis experiment to determine optimal concentration with dye 1 at high concentrations with 38  $\mu\text{M}$  bp DNA, and 10 mM sodium phosphate buffer, pH 7.0 irradiated with 741 nm light for 1 h in an ice bath at 10  $^{\circ}\text{C}$ . Lanes 1-4 are irradiated samples of dye 1 at 0, 12, 24, and 48  $\mu\text{M}$ , respectively and lanes 5-6 are dark controls.*

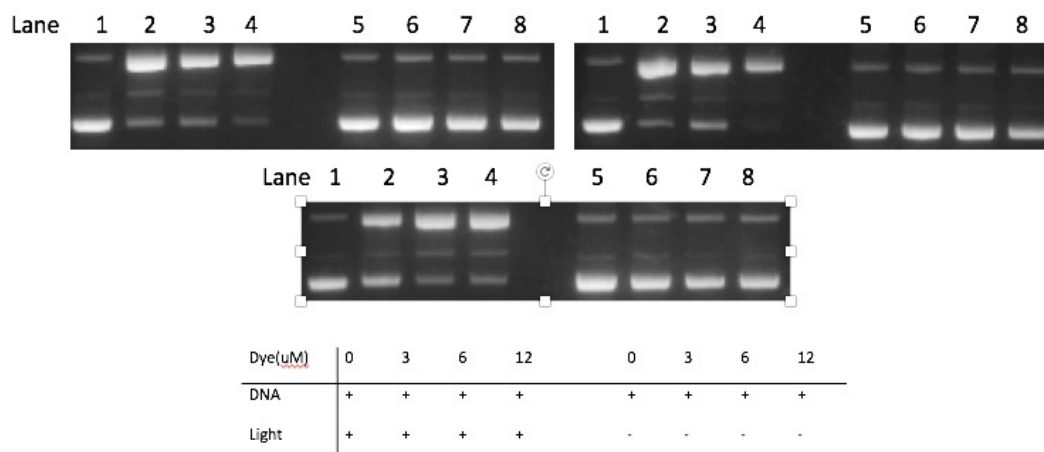
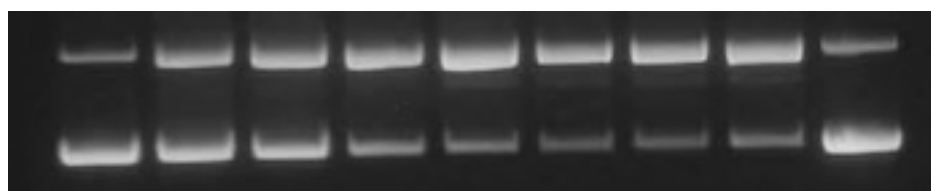
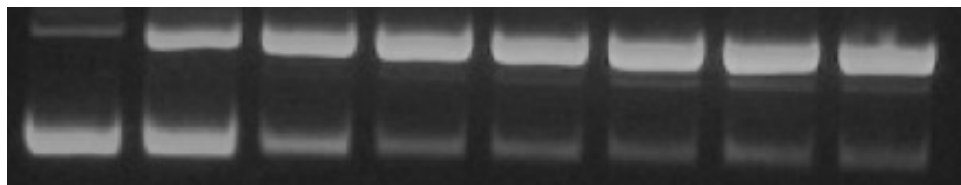


Figure 0.2 Gel electrophoresis experiment to determine optimal concentration with dye **1** at low concentrations with 38  $\mu\text{M}$  bp DNA, and 10 mM sodium phosphate buffer, pH 7.0 irradiated with 741 nm light for 1 h in an ice bath at 10  $^{\circ}\text{C}$ . Lanes 1-4 are irradiated samples of dye **1** at 0, 3, 6, and 12  $\mu\text{M}$ , respectively and lanes 5-8 are dark controls.



Lane	1	2	3	4	5	6	7	8	9
Dye	+	+	+	+	+	+	+	+	-
Time (min)	0	5	10	30	60	80	100	120	120
	85	73	63	40	24	18	12	11	94

Figure.0.3: Gel picture of photocleavage time course trial 2 with 24  $\mu\text{M}$  dye **1**, 38  $\mu\text{M}$  bp DNA, and 10 mM sodium phosphate buffer pH 7.0 with aliquots removed at  $t=0, 5, 10, 30, 60, 100,$  and 120 min at 25  $^{\circ}\text{C}$ . Lane 9 is a dark control.



	1	2	3	4	5	6	7	8
Dye	+	+	+	+	+	+	+	+
Time (min)	0	5	10	30	60	80	100	120
% supercoiled	92	66	20	10	7	4	4	4

*Figure 0.4 Gel picture of photocleavage time course trial 3 with 24  $\mu$ M dye 1, 38  $\mu$ M bp DNA, and 10 mM sodium phosphate buffer pH 7.0 with aliquots removed at  $t= 0, 5, 10, 30, 60, 100, \text{ and } 120$  min at 25  $^{\circ}$ C*

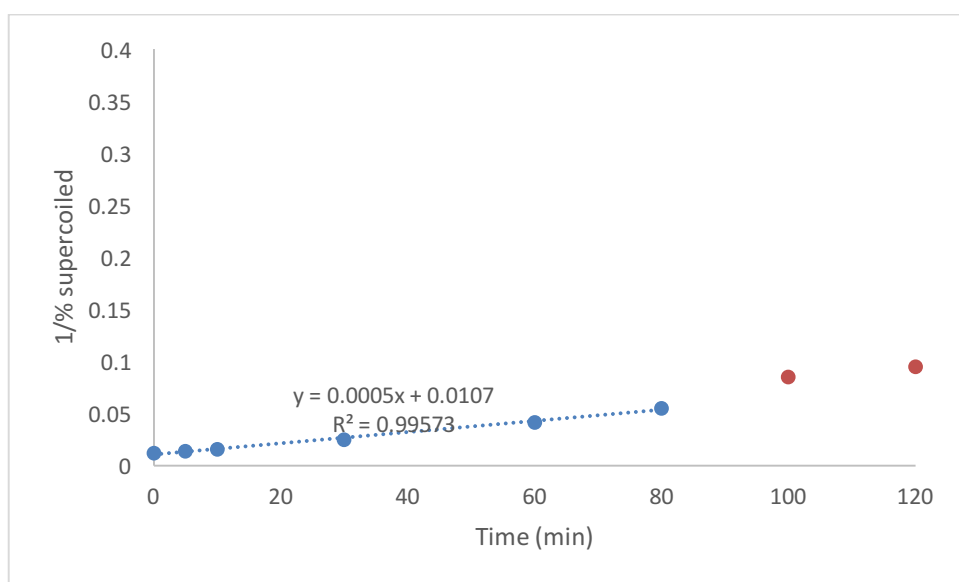
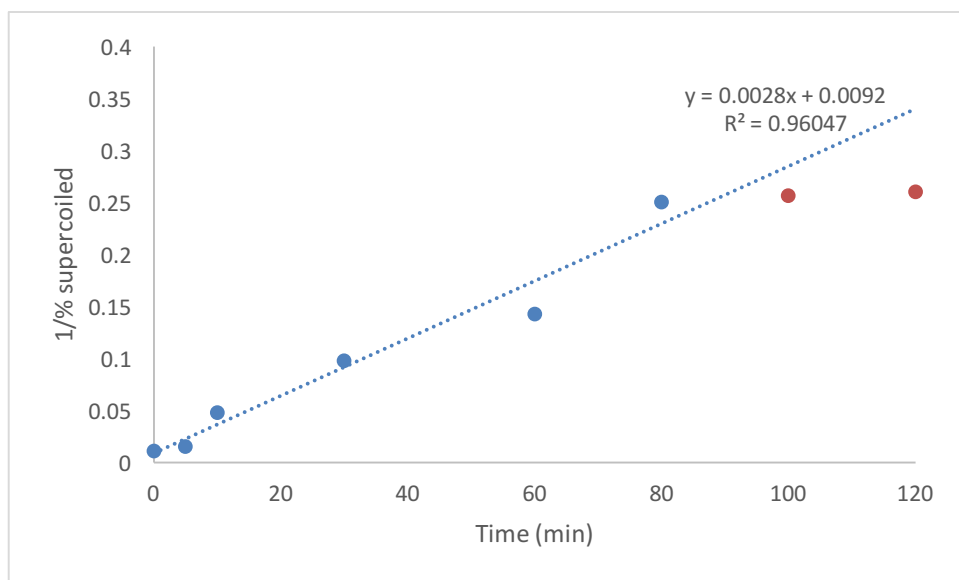
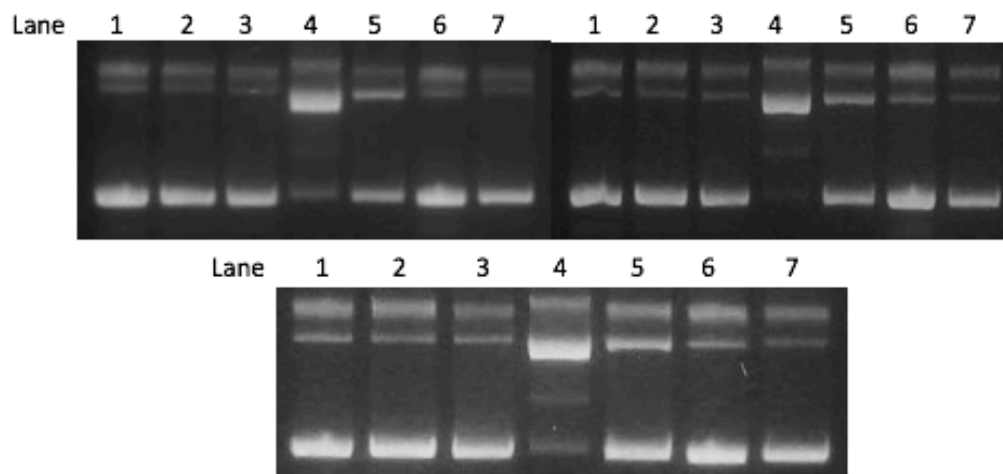
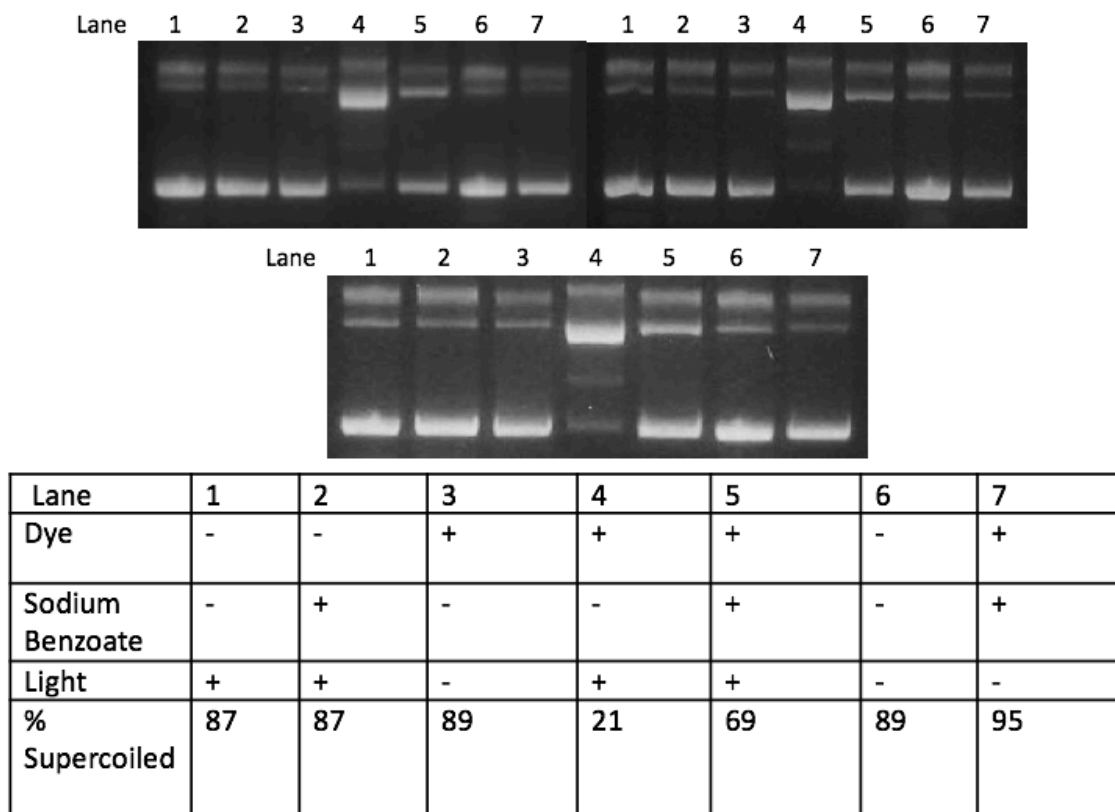


Figure 0.5 Second order kinetics plots trials 2 and 3 for  $24 \mu\text{M}$  dye **1** with  $38 \mu\text{M}$  bp DNA and  $10 \text{ mM}$  sodium phosphate buffer pH 7.0 at  $25 \text{ }^\circ\text{C}$ . Red data points were excluded from the curve fitting

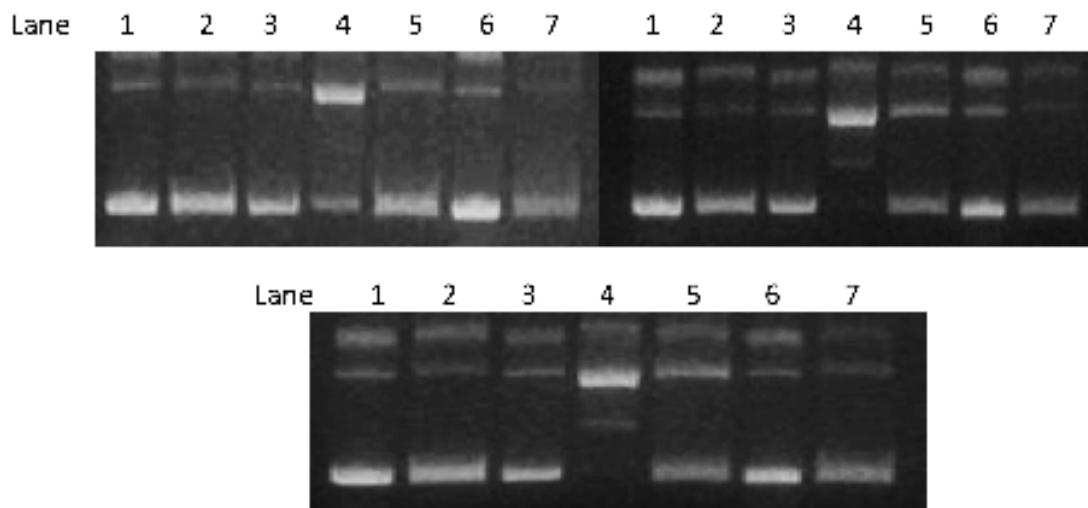


Lane	1	2	3	4	5	6	7
Dye	-	-	+	+	+	-	+
Sodium Azide	-	+	-	-	+	-	+
Light	+	+	-	+	+	-	-
% Supercoiled	87	87	89	21	69	89	95

*Figure 0.6 Sodium azide gel electrophoresis experiments with 24  $\mu\text{M}$  dye 1, 38  $\mu\text{M}$  bp DNA, 100 mM sodium azide, and 10 mM sodium phosphate buffer pH 7.0 irradiated at 741 nm with a 180 mW lamp for 1 h.*

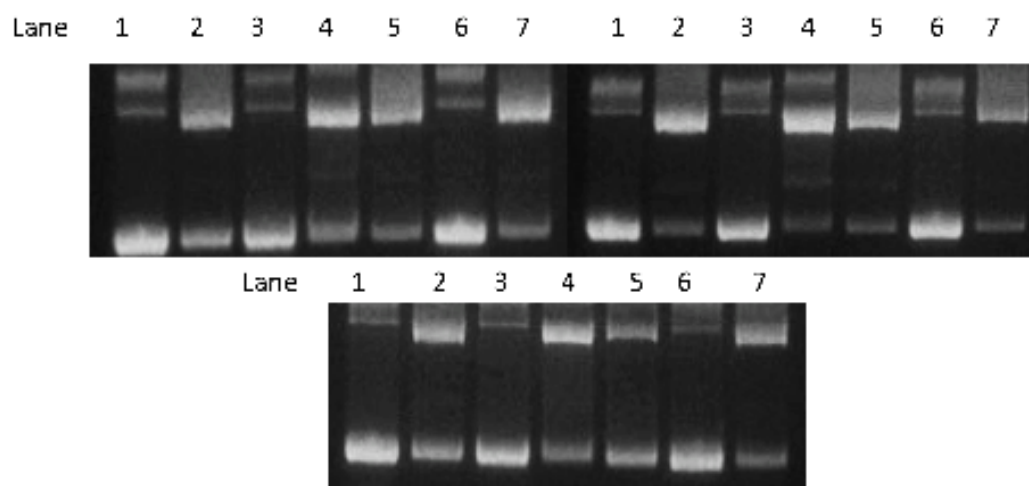


*Figure 0.7 Sodium benzoate gel electrophoresis experiments with 24  $\mu$ M dye 1, 38  $\mu$ M bp DNA, 100 mM sodium benzoate, and 10 mM sodium phosphate buffer pH 7.0 irradiated at 741 nm with a 180 mW lamp for 1 h*



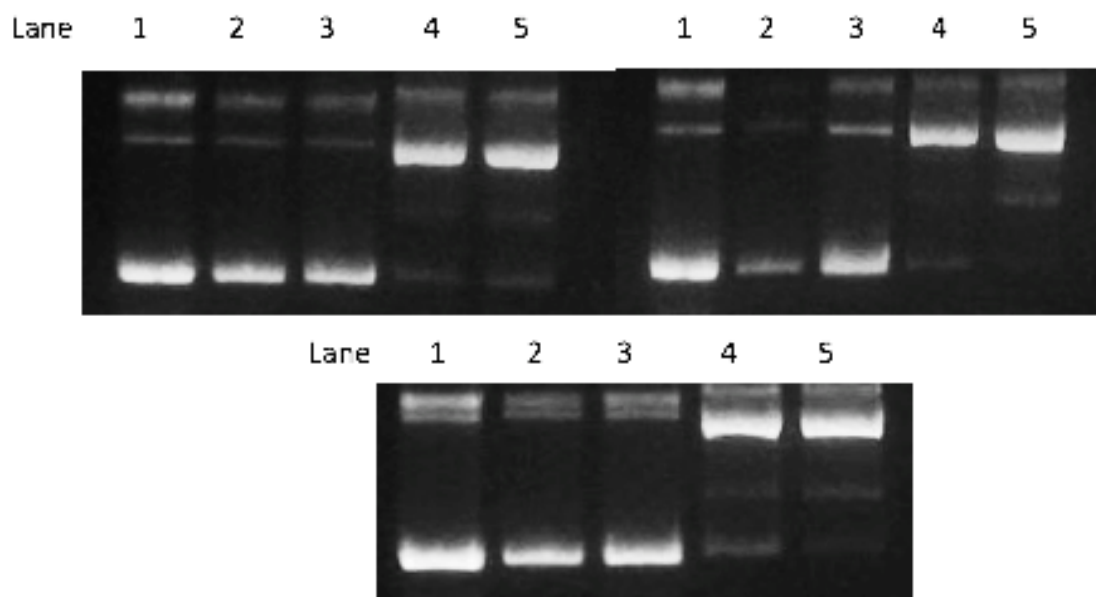
Lane	1	2	3	4	5	6	7
Dye	-	-	+	+	+	-	+
EDTA	-	+	-	-	+	-	+
Light	+	+	-	+	+	-	-
% supercoiled	88	87	77	10	50	81	85

*Figure 0.8 EDTA gel electrophoresis experiments with 24  $\mu\text{M}$  dye 1, 38  $\mu\text{M}$  bp DNA, 100 mM EDTA, and 10 mM sodium phosphate buffer pH 7.0 irradiated at 741 nm with a 180 mW lamp for 1 h*



Lane	1	2	3	4	5	6	7
Dye	-	-	+	+	+	-	+
Catalase	-	+	-	-	+	-	+
Light	+	+	-	+	+	-	-
% supercoiled	87	44	82	42	40	91	34

*Figure 0.9 Catalase gel electrophoresis experiments with 24  $\mu\text{M}$  dye 1, 38  $\mu\text{M}$  bp DNA, 100 U/ $\mu\text{L}$  catalase, and 10 mM sodium phosphate buffer pH 7.0 irradiated at 741 nm with a 180 mW lamp for 1 h*



Lane	1	2	3	4	5
Dye	-	+	+	+	+
D <sub>2</sub> O	+	-	+	+	-
Light	+	-	-	+	+
% supercoiled	87	89	68	7	12

*Figure 0.10 D<sub>2</sub>O gel electrophoresis experiments with 24  $\mu$ M dye 1, 38  $\mu$ M bp DNA, 72% (v/v) D<sub>2</sub>O, and 10 mM sodium phosphate buffer pH 7.0 irradiated at 741 nm with a 180 mW lamp for 1 h*